Upconversion Nanoparticles: Synthesis, Surface Modification, and Biological Applications

Meng Wang, PhD[a,c], **Mr Gopal Abbineni**[b], **April Clevenger, Ms**[b], **Chuanbin Mao, PhD**[b,*][Prof], and **Shukun Xu, Ms**[a,*][Prof]

[a] College of Sciences, Northeastern University, Shenyang 110819, P.R. China

[b] Department of Chemistry & Biochemistry, University of Oklahoma, 620 Parrington Oval, Room 208, Norman, Oklahoma 73019, U.S.A

[c] Shenyang National Laboratory for Materials Sciences, Institute of Metal Research, Chinese Academy of Sciences, Shenyang 110016, P.R. China

Abstract

New generation fluorophores, also termed upconversion nanoparticles (UCNPs), have the ability to convert near infrared radiations with lower energy into visible radiations with higher energy via a non-linear optical process. Recently, these UCNPs have evolved as alternative fluorescent labels to traditional fluorophores, showing great potential for imaging and biodetection assays in both in vitro and in vivo applications. UCNPs exhibit unique luminescent properties, including high penetration depth into tissues, low background signals, large Stokes shifts, sharp emission bands, and high resistance to photo-bleaching, making UCNPs an attractive alternative source for overcoming current limitations in traditional fluorescent probes. In this review, we discuss the recent progress in the synthesis and surface modification of rare earth doped UCNPs with a specific focus on their biological applications.

Keywords

upconversion; rare earth; luminescent materials; nanomaterials; biological detection

1. Introduction

Recent advancements in science have allowed a greater availability of enhanced sensitive analytical techniques, in particular, advanced tools for fluorescence imaging.[1] The last decade has provided a tremendous awareness regarding the use of fluorescent labeled molecules for cell and tissue labeling.[2] Despite the remarkable applicability of fluorescent dyes in imaging, their current use in visualizing mammalian cells is still greatly limited by the autoflourescence resulting from the excitation of fluorescent dyes. Thus, In order to meet the demands of modern technology, the development of next generation fluorescence probes is highly essential.[3]

Recent progress in nano-science has allowed scientists to develop new fluorescent nanoparticles (NPs) for biolabeling. These fluorescent labels are conjugated with biomolecules to generate detectable fluorescent signals used for investigating and understanding the complexity and dynamics of biological interactions at the molecular level.[4] In general, an ideal fluorescent probe should be ultra sensitive, resistant to photo-

Shukun Xu, xushukun46@126.com, Tel: 86-024-83681343. Chuanbin Mao, cbmao@ou.edu, Tel: 01-405-3254385.

bleaching, biocompatible, nontoxic and possess high fluorescent efficiency and superior chemical and physical stability.[3, 5]

In the last decade, organic dyes and fluorescent proteins have been the two most commonly used fluorescent probes for biological detections. Organic fluorescent dyes have several advantages over other fluorescent molecules as a result of their small size, good biocompatibity, easy surface modifications for covalent conjugations, and relatively high fluorescent intensity.[3] However; they are limited by short detection times due to high photo-bleaching efficiency and chemical degradation.[6] In addition, organic dyes often have narrow absorption and broad emission spectra with long tailing which limits their detection.[3, 6]

With the evolution of nanotechnology, semiconductor quantum dots (QDs) which possess size tunable emission, bright photoluminescence, good photo stability, broad ultraviolet (UV) excitation and narrow emission have emerged as alternative and promising fluorescent labels to conventional organic dyes.[7] These QDs have proven to have broad applications in areas such as fluorescence resonance energy transfer (FRET) analysis, gene delivery, cell labeling, and tissue imaging.[8] However, increasing concerns for QDs such as inherent cytotoxicity and chemical instability [9] have limited the employment of QDs to long term usage. Moreover, the excitation of traditional biolabels (organic dyes, fluorescent proteins and QDs) usually requires the use of UV or short wavelength radiation which results in serious limitations such as (i) low light-penetration depth inherent to the short wavelength excitation light, (ii) possible damage or even death of biomolecules caused by long-term irradiation, and most importantly, (iii) low signal-to-noise ratio due to significant autofluorescence (background) from biological samples in the UV short wavelength regions.

Therefore, it is highly essential to develop more efficient biolabels to overcome the limitations of traditionally used biolabels. Recently, the conversion of near infrared radiations into visible light via non-linear optical processes, termed upconversion (UC), has generated great interest from researchers. Currently, applications of upconversion nanoparticles (UCNPs) have become very prominent in the medical field. In particular, Rare earth (RE) doped near infrared (NIR)-to-visible UCNPs serve as an alternative and excellent substitute for traditional fluorescent labels.

RE doped UCNPs, which can convert long wavelength radiation (*e.g.*, NIR light) into short wavelength fluorescence (*e.g.*, visible light) via a two-photon or multi-photon mechanism,[10] is emerging as a new class of fluorescent biolabels.[11–15] Distinguished from traditional fluorescent biolabels, RE doped UCNPs can be excited by NIR radiation and possesses several advantages which include (i) an excellent signal-to-noise ratio and improved detection sensitivity owing to the absence of autofluorescence, (ii) deeper NIR light penetration into biological tissue causing less photo damage to biological samples, and (iii) excitation via a low power NIR laser which is compact and inexpensive.[11–15] Additional advantages of UCNPs include narrow emission peaks, large Stokes shifts, good chemical and physical stability, and low toxicity.[5] Therefore, RE doped UCNPs are very promising alternatives to traditional fluorescent biolabels for potential medical applications.

The main purpose of this review is to provide insight into the recent progress of the synthesis, surface modification, and biological applications of RE doped UCNPs. The challenges and perspectives of these UCNPs are also discussed at the end of this review.

2. Properties of upconversion nanoparticles (UCNPs) and rare earth (RE) doped UCNPs

2.1. Principle and types of Upconversion (UC) processes

The process of UC has been extensively studied in the past few years and has proven to be a successful method for generating visible light from NIR radiation. UC is a non-linear optical process by which excitation of lower electronic levels with low energy radiation (NIR light) results in higher energy emission (visible or UV light) at higher electronic levels, and can therefore be ascribed as an anti-Stokes mechanism. This process requires the absorption of two or more photons to provide the sufficient energy for the UC emission to occur. There are three different classes of UC processing mechanisms which can lead to the two or more photon absorption: excited state absorption, energy transfer, and photon avalanche.[16]

2.1.1. Excited state absorption (ESA)—Excited state absorption (ESA), also known as sequential two-photon absorption, is one of the most accepted models of UC, proposed by Bloembergen in 1959.[17] ESA involves the absorption of photons via a single ion, and is the only UC process which occurs in materials with a low dopant concentration. The general energy scheme of ESA is shown in figure 1 and involves the successive absorption of two photons. The first photon causes an ion from the ground state (state 1) to enter a long-lived intermediate excited state (state 2), known as the ground state absorption (GSA). A second photon then promotes this ion from state 2 to the higher excited state (state 3) in optical transition and results in UC emission.

2.1.2. Energy transfer—UC via energy transfer (ET) between excited ions was studied extensively in the mid 1960's. The pioneering contributions of Auzel resulted in the observation of the ATPE (addition de photons par transfert d'energie) effect,[18] which was later termed energy transfer (ET) UC. Distinguished from the ESA process, the ET process involves a sequential absorption of two photons that transfer energy from an excited ion (sensitizer or donor) to another neighboring ion (activator or acceptor), and is observed in materials with high dopant ion concentrations. There are different types of well known ET mechanisms including ET followed by ESA (EFE), successive energy transfer (SET), cross relaxation (CR), cooperative sensitization (CS), and cooperative luminescence (CL) which are listed in Table 1.

2.1.3. Photon avalanche—A photon avalanche (PA), also known as an absorption avalanche, is among the most efficient types of UC which was first discovered by Chivian in 1979.[19] The PA process is the least observed among all the UC schemes involving an ESA of incident light as well as intrinsic CR. Figure 2 shows the most simple energy scheme for a PA process.

Initially, the sensitizing ion (ion 1) in state 1 is promoted to its state 2 by ground state absorption (GSA). Next, an incident photo promotes it to its state 3 via an ESA. The fundamental nature of the PA process is that one sensitizing ion (ion 1) in state 3 can interact with a neighboring ion (ion 2) in the ground state to produce two ions (ion 1 and 2) in state 2 as a result of CR. The two resultant ions act as sensitizing ions which can produce an additional four ions, which in turn can produce another eight *etc.*. Eventually the intermediate excited state (state 2) acts as a storage reservoir for energy so that an avalanche of the ion population in state 2 can be established.

2.2. RE doped UCNPs

Recently, RE doped UCNPs have gained considerable attention because of their unique ability to emit light with higher energy than the excitation wavelength. In most cases, RE

doped UCNPs are composed of three components: a host matrix, sensitizer, and activator.[11] Host matrix is one of the most important components of UCNPs as they provide essential and unique UC optical properties including UC efficiency and emission profile. Sensitizer can be excited effectively from the energy of the incident light source which transfers this energy to the activator where radiation can be emitted. Therefore, activator is the luminescence center in UCNPs while the sensitizer enhances the UC luminescence efficiency. The dopants, sensitizer and activator are added to the host lattice in relatively low concentrations (usually ~20 mol% for the sensitizer and <2 mol% for the activator).

In general, all trivalent RE ions exhibit similar ionic sizes and chemical properties. In addition, their inorganic compounds provide an ideal host matrix for UCNPs. Host matrixes with low lattice photon energies, however, are required to minimize the non-radiative loss and maximize the radiative UC emission. The trivalent Yb^{3+} ion, having an extremely simple energy level scheme, is suitable for use as a UC sensitizer. Most RE^{3+} ions (except La^{3+}, Ce^{3+}, Yb^{3+}, and Lu^{3+} ions) have more than one excited level and are suitable for acting as UC activators. Er^{3+}, Tm^{3+}, and Ho^{3+} ions have energy levels in the form of a ladder and hence are most frequently used as UC activators. Table 2 shows several types of known UCNPs as well as their luminescent properties (under 970–980 nm NIR excitation).

2.3. RE doped NaYF$_4$ UCNPs

Among the available different types of UC host materials, fluorides have proven to be ideal host candidates for UC because of their very low phonon energies and high chemical stability. In particular, Yb^{3+}/Er^{3+} and Yb^{3+}/Tm^{3+} doped $NaYF_4$ have been previously reported as the most efficient UC materials for giving green and blue emissions.[51, 52] Recently, Liu's group along with other have focused on the synthesis, surface modification, and biological applications of RE doped $NaYF_4$ UCNPs.[11–15, 53]

There are two types of crystalloid phases that exist in $NaYF_4$ at ambient pressure: the cubic phase (α-phase) and the hexagonal phase (β-phase).[54] It has been reported that the more thermodynamically stable, β-$NaYF_4$, can be transformed from the α-$NaYF_4$. Interestingly, the $NaYF_4$ phase we often obtained was the thermodynamically meta stable α-phase rather than the stable β-phase. That is due to the fact that the free-energy barrier for the conversion from α-$NaYF_4$ to β-$NaYF_4$ is very high, requiring more energy for the transition from the cubic-to-hexagonal phase.[55] In most cases, β-$NaYF_4$ can be obtained via a heating treatment such as annealing, hydrothermal or solvothermal treatments, often requiring harsh conditions with high reaction temperatures and long reaction times.

The UC intensity of RE doped $NaYF_4$ is closely related to its phase where the UC efficiency of β-$NaYF_4$ is much higher than that of α-$NaYF_4$. For example, the green emission of β-$NaYF_4$:Yb,Er is 10 times stronger than that of α-$NaYF_4$:Yb,Er and the overall (green plus red) emission of the former is 4.4 times higher than that of the latter. Thus, in order to overcome the current limitations of traditional fluorescent probes in biological applications, RE doped β-$NaYF_4$ UCNPs are appropriate substituents due to their superior UC properties.

3. Synthesis and formation mechanism of RE doped NaYF$_4$ UCNPs

3.1. Coprecipitation method

The coprecipitation method is one of the easiest and most convenient approaches for synthesizing RE doped $NaYF_4$ UCNPs because of their mild reaction conditions, low costs for required equipment, simple protocols, and short reaction times. Yi et al.[56] firstly reported the coprecipitation method in synthesizing $NaYF_4$:Yb,Er UCNPs with the aid of ethylenediamine tetraacetic acid (EDTA). In this procedure, Yi et al. quickly injected an RE-EDTA complex into a NaF solution while stirring vigorously. This resulted in the

formation of α-NaYF$_4$:Yb,Er UCNPs through a homogeneous nucleation process. The sizes of the resulting UCNPs can be controlled from 37 to 166 nm by varying the molar ratio of EDTA to the total RE^{3+} ions. Because the resulting UC fluorescent intensity of the α-NaYF$_4$:Yb,Er UCNPs was too weak to be applied to biological labeling, an annealing treatment was used to enhance the UC fluorescent intensity. This resulted in the phase transition from a cubic-to-hexagonal phase, thereby increasing the fluorescent intensity of the UCNPs by up to 40-fold.

However, after annealing, the UCNPs tended to aggregate into larger sizes at higher temperatures (above 400 °C), which limited their potential applications. Later, Wei et al.[57] reported a similar method to synthesize NaYF$_4$:Yb,Tm UCNPs in the presence of EDTA. Their studies showed that changes in pH greatly affected the morphology of the resulting NPs. For example, the particles tended to aggregate when the pH value was 10.0, and began to form fibroid like structures when the pH value was increased to 12.0. The differential scanning calorimetric (DSC) experiments and analysis showed that EDTA molecules capped on the surface of the NPs could suppress the cubic-to-hexagonal phase transition, prohibiting transformation from the α-phase to β-phase of the NPs even when annealed at 600 °C for 5 h.

For the synthesis of RE doped NaYF$_4$ UCNPs by the coprecipitation method, post-heat treatment (annealing) is typically required to promote UC fluorescent intensity which in turn allows the NPs to aggregate and become larger. Since annealing with capping reagents such as EDTA can become carbonized after the annealing process, reducing the hydrophilicity of the NPs, further surface modifications such as surface silica coating is often required to improve the hydrophilicity of the NPs to allow further increasing of NP size. Therefore, the application of RE doped NaYF$_4$ UCNPs synthesized via the coprecipitation method in biological field is limited.

3.2. Thermal decomposition method

Since metallic trifluoroacetates can thermally decompose to their corresponding metal fluorides, Zhang et al.[58] first reported a novel synthesis of single-crystalline and monodisperse LaF$_3$ triangular nanoplates via the thermal decomposition of lanthanum trifluoroacetates (La(CF$_3$COO)$_3$). Since its discovery, this method has become a common route for synthesizing high quality RE doped NaYF$_4$ UCNPs.

Mai et al.[55] reported a general synthesis of high-quality (monodisperse, single-crystalline, well-shaped and phase-pure) NaREF$_4$ (RE = Pr to Lu, Y) NPs using Na(CF$_3$COO) and RE(CF$_3$COO)$_3$ as precursors. The combined solvents were composed of both the coordinating solvent and non-coordinating solvent. 1-octadecene (ODE) with a high boiling point (315 °C) was used as the non-coordinating solvent to provide a high temperature environment. Oleic acid (OA) and oleyamine (OM), having good coordinate abilities, acted as the coordinating solvent which aids in capping the surface of NPs to prevent agglomeration. From a series of experiments, they demonstrated that pure β-NaYF$_4$ could be prepared from the OA-ODE system under harsh conditions (high Na/RE ratio, high temperature, and long reaction time), while pure α-NaYF$_4$ could be obtained from the OA-OM-ODE system under relatively mild conditions (low Na/RE ratio, low temperature, and short reaction time). These methods allowed the successful synthesis of high quality α- and β-phase NaYF$_4$:Yb,Er/Tm UCNPs.

Boyer et al.[59] also reported a similar procedure to synthesize α-NaYF$_4$:Yb,Er/Tm UCNPs using Na(CF$_3$COO) and RE(CF$_3$COO)$_3$ as precursors, however, the particle size distribution resulted in a broad range (10–60 nm). They slowly added the dissolved precursors to the reaction solution which resulted in monodisperse α-NaYF$_4$:Yb,Er/Tm UCNPs with narrow

size distributions (22–32 nm).[60] They showed that the rate of decomposition and particle formation could be controlled via the addition of precursors to the reaction solution over a long period of time. Thus, the nucleation and growth stages of the NPs could be separated resulting in monodisperse NPs with narrow distributions. However, it is still necessary to understand the detailed mechanism of size and phase controlled synthesis of UCNPs.

Mai et al.[61] found that the UC emission (the intensity and ratio of green to red emission) was sensitive to the growth process (nucleation and phase transition process) of $NaYF_4$:Yb,Er UCNPs and provided a powerful tool for investigating the growth and phase transition stages of NPs. In their studies, they demonstrated that $NaYF_4$:Yb,Er UCNPs synthesized by the thermal decomposition of precursors, were formed via a unique delayed nucleation pathway in a solution phase. In addition, monodisperse β-$NaYF_4$:Yb,Er UCNPs with tunable sizes could be obtained from α-$NaYF_4$:Yb,Er monomers by restricting or enhancing the Ostwald-ripening process in which the cubic-to-hexagonal phase transition process happened in a delayed time. This method was later developed as a common route to synthesize other kinds of NPs.

Ehlert et al.[62] have developed a series of RE doped $NaYbF_4$ UCNPs via a typical thermal decomposition method. More interestingly, the Er^{3+}, Tm^{3+} and Ho^{3+} ion doped $NaYbF_4$ UCNPs could produce red, blue and green light under a 980 nm radiation, respectively, showing their potential use in multiplex analysis. In another example, Du et al.[63] reported the synthesis of $NaMF_3$ (M = Mn, Co, Ni, Mg) and $LiMAlF_6$ (M = Ca, Sr) nanocrystals using a similar approach. It should be noted that $NaMgF_3$:Yb,Er nanorods with the size of $(337.2 \pm 66.3) \times (10.3 \pm 1.6)$ nm^2 synthesized by Du et al. was the first report to show a strong red emission under 980 nm radiation.

More recently, Shan et al.[64] reported a new thermal decomposition method for the synthesis of monodisperse β-$NaYF_4$:Yb,Er/Tm/Ho UCNPs using a single solvent (trioctylphosphine oxide, TOPO) rather than the previously mentioned component solvent (OA/ODE or OA/OM/ODE). Here, TOPO was used as a boiling solvent and capping reagent to control crystalline growth by providing a broad temperature window for the synthesis of β-$NaYF_4$:Yb,Er/Tm/Ho UCNPs. The as-prepared UCNPs were small in particle size (~10 nm) with a high UC efficiency and narrow size distribution. They demonstrated that the energy barrier of the cubic-to-hexagonal phase transition process was significantly reduced using TOPO allowing more efficient formation of β-phase UCNPs. Later, they reported a similar synthesis of β-$NaYF_4$:Yb,Er UCNPs using ODE and the combined capping reagents of OA and trioctylphosphine (TOP). The kinetic mechanisms for the particle phase transition and growth were discussed in detail.[65] From a series of experimental results, they proposed that the formation of β-phase UCNPs could be divided into two stages: firstly, a kinetic controlled precipitation stage for the formation of α-phase UCNPs, and secondly, the diffusion controlled growth and size focusing stage for the formation of β-phase UCNPs. They also found that the UC intensity was proportional to the size of the β-phase UCNPs.

Chen et al.[66] reported a novel thermal decomposition method for synthesizing α- and β-phase $NaYF_4$:Yb,Er UCNPs using RE-oleate complexes as the precursors and ODE as the reaction solvent. This could also be attributed to a liquid-solid two-phase approach. By adjusting the reaction temperature, α-$NaYF_4$:Yb,Er UCNPs could be obtained at 210 °C for 6 h, and β-phase UCNPs could be prepared at 260 °C for 6 h which is relatively milder than other thermal decomposition methods mentioned above.

Although the thermal decomposition method has proven to be an effective approach for fabricating monodisperse, single-crystalline, well-defined, and phase-pure UCNPs, there remains some disadvantages such as required rigorous (anhydrous and oxygen-free) and

harsh (long reaction time and high reaction temperature) synthesis conditions. In addition, the thermal decomposition of the metal trifluoroacetates produces fluorinated and oxy-fluorinated carbon species which are considered to be toxic. More importantly, the capping ligands such as OA, OM, and TOPO bind to the surface of NPs via outward hydrophobic alkyl chains, rendering the NP surface hydrophobic. This limits the use of these UCNPs for biological applications in which further surface modifications are essentially required.

3.3. Hydrothermal/solvothermal method

The hydrothermal/solvothermal method refers to a chemical synthesis procedure within a sealed environment under high pressure and temperature (often above the critical point of the solvent). In a typical hydrothermal/solvothermal synthesis, specialized reaction vessels known as autoclaves are often used to provide the sealed reaction environment.

Sun et al.[67] reported a hydrothermal synthesis of α- and β-phase $NaYF_4$:Yb,Er UCNPs using RE-EDTA or RE-citrate complexes as precursors. EDTA and citrate were used as capping ligands to control the size and morphology of the NPs. They found that the particle size was dependent on the nucleation rate which could be controlled by the concentration of the reactants, molar ratio of RE, capping ligands to NaF, and choice of capping ligands. There are several examples for the hydrothermal synthesis of high-quality UC micro/nanoparticles using EDTA or citrate as capping reagents.[68–74]

Liang et al.[75] also reported a solvothermal synthesis of branched $NaYF_4$:Yb,Er UCNPs in the presence of cetyltrimethylammonuim bromide (CTAB) in a methanol-water system. Here, CTAB was used as a regulating reagent to facilitate the branched growth of NPs. Due to its unique structure, these branched $NaYF_4$:Yb,Er UCNPs could be introduced into polystyrene to form a novel multifunctional polymer which showed green excitation emissions under 980 nm. Zeng et al.[76] reported a solvothermal synthesis of β-$NaYF_4$:Yb,Er UCNPs in selected solvents (water, acetic acid or ethanol) with the aid of EDTA and CTAB. In their studies, the size and morphology of the NPs were controlled via EDTA and CTAB, respectively. EDTA possesses excellent chelating abilities that can reduce particle size and CTAB acts as a surfactant for tuning the morphology of nanocrystals from nanoparticles to nanorods. Later, EDTA-CTAB was used to aid the solvothermal method developed by Zeng et al.[77] as a general synthesis route for preparing complex RE fluoride NPs such as $NaYF_4$:Yb,Er/Tm, $NaGdF_4$:Eu, and $NaCeF_4$ NPs.

Wang et al.[78] developed a one-step synthesis of polyethylenimine (PEI) coated $NaYF_4$:Yb,Er/Tm UCNPs via a solvothermal approach. This was the first report made on the one-step synthesis of water-soluble and biocompatible $NaYF_4$:Yb,Er/Tm UCNPs. PEI, an organic polymer surfactant, was used in this study to control the particle size and prevent particle aggregation. More importantly, the free amine groups on the surface of the UCNPs could bind with biomolecules (such as antibodies), facilitating the use of UCNPs in biological applications. They also demonstrated that the PEI coated UCNPs were biocompatible with mammalian cells. Later, they reported a similar approach for synthesizing PEI-coated $NaYF_4$:Yb,Er/Tm UCNPs using ethylene glycol as the reaction solvent.[79] Interestingly, they developed three-component (Yb, Er, Tm) doped $NaYF_4$ UCNPs. After fine-tuning by adjusting the amount of dopants, these UCNPs could emit multi-colors ranging from blue to white which has great potential uses for multiplexed labeling.

Wang et al.[80] developed a novel liquid-solid-solution (LSS) strategy for the synthesis of NPs which exhibited semiconducting, fluorescent, magnetic, and dielectric properties. This LSS strategy involved two main processes called phase transfer and phase separation and was further developed as an effective way to synthesize RE fluoride NPs[78, 81] including RE

fluoride UCNPs.[82] Later, Wang et al.[83] reported a solvothermal synthesis of monodisperse $NaYF_4$:Yb,Er single-crystal nanorods, hexagonal nanoplates, and nanoparticles using the LSS synthetic strategy. From the experimental results, they indicated that high NaF content, low RE^{3+} content, appropriate temperatures, and long reaction times could facilitate the epitaxial growth of $NaYF_4$:Yb,Er NPs.

Our group, Wang et al.[42] reported a two-phase solvothermal synthesis of $NaYF_4$:Yb,Er/Tm/Ho UCNPs in a water-ethanol-oleic acid system (Figure 3). In their studies, RE stearate was first used as the precursor. Later, they developed a one-step synthesis of polymer coated $NaYF_4$:Yb,Er UCNPs by employing a series of polymers such as polyvinylpyrrolidone (PVP), polyethylene glycol (PEG), polyacrylic acid (PAA), and polyethylenimine (PEI) rather than oleic acid.[84] These polymers which were capped on the surface of the UCNPs, proved highly important as they made the NPs hydrophilic and prevented them from aggregating.

The advantages for adopting a hydrothermal/solvothermal method for synthesizing high quality UCNPs include (i) a high purity of product, (ii) easy control of size, structure, and morphology of the NPs, (iii) relatively lower reaction temperatures (in general below 200 °C),[85] and (iv) simple equipment and overall process.[86] However, in most cases, the hydrophilicity of UCNPs prepared using the hydrothermal/solvothermal method was not sufficient due to the presence of hydrophobic organic ligands (such as oleic acid) on the surface of the NPs. Therefore, to improve the water-solubility and biocompatibility of the UCNPs, surface modifications are a high priority.

3.4. Other methods

Polyols which have high boiling points and good water-solubility, have widely been used as solvents for preparing different varieties of NPs including metals,[87] oxides,[88] and phosphates.[89] Wei et al.[90] reported a polyol method for preparing $NaYF_4$:Yb,Er/Tm UCNPs. In their studies, three kinds of polyols which included ethylene glycol, diethylene glycol, and glycerol were used not only as solvents but also as capping ligands for limiting the growth of NPs and stabilizing them from aggregation. After the solvothermal procedure, the phase of the UCNPs was converted from the α-phase to β-phase resulting in an enhancement of the fluorescent intensity. Since polyols are water soluble, the as-prepared UCNPs could be well dispersed in water. Other kinds of fluorides such as $NH_4Y_3F_{10}$ and YF_3 were also synthesized using this polyol-mediated method.[91]

Li et al.[92] reported a simple and user-friendly method for the synthesis of β-$NaYF_4$:Yb,Er/Tm UCNPs with enhanced fluorescence. This system has two major steps: the first, nucleation at room temperature and the second, particle growth at elevated temperatures (300 °C). Similar to typical thermal decomposition methods, OA and ODE were used in this method to provide a high-temperature environment for the cubic-to-hexagonal phase transition. Here, the use of metal trifluoroacetates was avoided to limit the toxicity of fluorine species. However, use of rigorous synthetic conditions involving anhydrous and oxygen free environments were still required.

Heer et al.[93] reported a three-step synthesis of $NaYF_4$:Yb,Er/Tm UCNPs using N-(2-hydroxyethyl)-ethylenediamine (HEEDA), a high boiling organic solvent. This method involved the preparation and reaction of two educt-solutions (containing Na^+ and RE^{3+} cations, and F^- anions, respectively) in HEEDA. The resulting UCNPs were dispersed in dimethyl sulfoxide (DMSO) to form a transparent colloidal solution. This method is the first reported synthesis of $NaYF_4$:Yb,Er/Tm UCNPs.

4. Modification of RE doped NaYF$_4$ UCNPs

In general, RE doped NaYF$_4$ UCNPs synthesized using the above mentioned methods are not water soluble due to the presence of hydrophobic organic ligands such as oleic acid on the surface of the NPs. In most cases, even if the NPs are water dispersible, there are no appropriate functional groups (such as carboxyl groups or amino groups) on the surface of the NPs. Therefore, the conjugation between the UCNPs and biomolecules becomes difficult for practical biomedical applications. To overcome this problem, further surface modifications are necessary. The surface modification of the UCNPs can be achieved in two ways: (i) surface modification with an inorganic shell layer, and (ii) surface modification with organic capping ligands.

4.1. Surface modification with an inorganic shell layer

In most cases, surface modification with an inorganic shell layer is achieved via surface silanization. In this procedure, the surfaces of synthesized NPs are further coated with amorphous silica. A well-known Stober procedure which involves the hydrolysis and condensation of siloxane precursors such as tetraethoxysilane (TEOS) in the presence of ethanol and ammonia, has been widely used for the surface silanization of UCNPs.[94]

A good example of coating the surface with silica was reported by Li *et al.*, who coated polyvinylpyrrolidone (PVP) stabilized NaYF$_4$:Yb,Er/Tm UCNPs with a layer of silica via a typical Stober method as shown in Figure 4.[95] In their studies, the thickness of the silica shell was approximately 10 nm and could be controlled within 1–3 nm by adjusting the initial amount of TEOS taken. After coating with silica, the UCNPs were quite stable in water and still emitted strong UC fluorescence. The use of Stober method to coat silica is not only limited to UCNPs synthesized via the hydrothermal/solvothermal method but is also applicable to UCNPs prepared via the thermal decomposition method. Shan *et al.*[96] modified the NaYF$_4$:Yb,Er UCNPs synthesized in hydrophobic organic solvents (OA-ODE and OA-TOP-ODE) with a layer of silica using a Stober-based microemulsion reaction. However, the silica-coated NPs tend to be aggregate when removed from the microemulsion. Later, Johnson *et al.*[97] reported a facile method to solve this problem. They changed the OA-coated hydrophobic NaYF$_4$:Yb,Er UCNPs to hydrophilic, which involved a ligand exchange between OA and PVP, and then modified the PVP-stabilized UCNPs with a layer of silica. The results show that the resultant silica-coated NPs have a higher colloidal stability and a better monodispersity, compared with the NPs prepared in reverse microemulsion.

Recently, Li *et al.*[98] reported a novel surface modification combined with the fluorescence resonance energy transfer (FRET) mechanism to generate multicolor silica-coated UCNPs. In their work, some organic dyes or QDs were first encapsulated together with NaYF$_4$:Yb,Er or NaYF$_4$:Yb,Tm UCNPs, respectively, using a Stober-based microemulsion method. When excited by a 980 nm radiation, the UC fluorescence emitted from the UCNPs (core) was transferred to the organic dyes or QDs (shell) via a FRET process, thus, different colors could be generated using different organic dyes or QDs (Figure 5). These multicolor NPs have great potential in multiplexed bioassays.

Even though coating the surface of NPs with silica allows them to be water dispersible, it may not provide the required functional groups for bioconjugation. To solve this problem, the hydrolysis of amino siloxanes such as (3-aminopropyl)triethoxysilane (APS) are often performed to generate functional amino groups on the surface of the silica coated NPs.

Recently, synthesis of multi-functional NPs have drawn a great deal of attention.[99] Lu *et al.*[100] reported the synthesis of NaYF$_4$:Yb,Er core-shell UCNPs with multi functional

capabilities including magnetic, fluorescent, and bioaffinity properties. In this procedure, they used iron oxide NPs as a magnetic core covered by a layer of $NaYF_4$:Yb,Er via a coprecipitation method. After annealing, the fluorescence intensity of the NPs was greatly enhanced. The resulting NPs were then coated with silica and amino-functionalized by the hydrolysis of TEOS and APS which rendered the UCNPs water-soluble and biocompatible (Figure 6).

Liu et al.[101] also reported a synthesis of superparamagnetic $NaYF_4$:Yb,Er core-shell UCNPs. In their synthesis, $NaYF_4$:Yb,Er UCNPs together with Fe_3O_4 superparamagnetic NPs acted as a core and were encapsulated in a silica shell via the hydrolysis of TEOS and APS in a reverse microemulsion system. These biocompatible NPs exhibited both UC fluorescence and magnetic properties and are emerging as promising materials for bioimaging, drug targeting, and bioseparation.

Likewise, Mi et al.[102] have recently reported that active functional groups on the surface of Fe_3O_4/NaYF4:Yb,Er magnetic/luminescent nanocomposites can be used to be successfully conjugated to antibodies to recognize mammalian cells. In their recent paper, Mi et al. have successfully conjugated trasferrin protein on to luminescent nanocoposites and were able to specifically recognize the transferrin receptors which were over expressed on HeLa cells.

4.2. Surface modification with organic capping ligands

Schafer et al.[103] reported the first synthesis of $NaYF_4$:Yb,Er/Tm UCNPs in HEEDA, and further modified the surface with an organic ligand, namely, 1-hydroxyethane-1,1-diphosphonic acid (HEDP). After surface modification, the resulting $NaYF_4$:Yb,Er/Tm UCNPs were water soluble, These UCNPs were further purified by the removal of HEEDA which resulted in an increased UC efficiency. This method, however, required high temperatures (180 or 320 °C) and a vacuum ($p < 0.1$ mbar).

Yi et al.[104] reported the synthesis of oleyl amine (OM) stabilized β-$NaYF_4$:Yb,Tm UCNPs via a typical thermal decomposition method. The hydrophilic amino groups of OM could bind to the surface of the UCNPs while the hydrophobic alkyl chains extended outward resulting in a hydrophobic NP surface. Later, they changed the hydrophobic surface to hydrophilic using a bipolar surfactant, polyethylene glycol 600 diacid (PEG600 diacid), which involved a ligand exchange between OM and PEG600 diacid. In the ligand exchange process, the carboxyl group on one end of PEG600 diacid was capped onto the surface of the UCNPs while the carboxyl group on the other end extended outward, making the UCNPs more hydrophilic (Figure 7a). After the ligand exchange, the NPs could be dispersed in water to form a clear and stable colloid solution for at least two weeks. The free carboxyl groups on the surface of the UCNPs are of great importance for further conjugation with biomolecules. Zhang et al.[105] also reported a similar ligand exchange approach for converting the OM modified $NaYF_4$:Yb,Er/Tm UCNPs from hydrophobic to hydrophilic using hexane diacid as the modifier. Boyer et al.[106] changed the hydrophobic OA-coated $NaYF_4$ NPs to hydrophilic by the aid of PEG-phosphate ligands via a ligand exchange process, and then coated the resultant NPs with a silica shell to avid the luminescent quenching effect of the NPs in aqueous environments.

Later, Yi et al.[107] reported another method for modifying the surface of OM stabilized β-$NaYF_4$:Yb,Er/Tm $NaYF_4$ core-shell UCNPs via a ligand attraction process. In their studies, the β-$NaYF_4$:Yb,Er/Tm core was first coated with a $NaYF_4$ shell to enhance the UC fluorescence intensity of the NPs. Then, an amphiphilic layer, 25% octylamine and 40% isopropylamine modified polyacrylic acid (PAA), was used as the modifier to make the UCNPs hydrophilic. This process involved hydrophobic interactions between the alkyl chains, the octyl on the surfaces of the NPs and the octyl and isopropyl groups in the

modified PAA molecules (Figure 7b). After achieving surface modification, the hydrophilic carboxyl groups of the modified PAA extended outwards which made the NPs water-soluble, facilitating their attachment to biomolecules. This method is suitable for UCNPs with hydrophobic functional groups on the surface.

Based on the fact that a carbon-carbon double bond can be oxidized directly to form two carboxyl groups with the aid of a Lemieux-von Rudloff reagent ($KMnO_4$ and $NaIO_4$ aqueous solution), Chen *et al.*[108] developed a novel ligand oxidation method for modifying OA stabilized $NaYF_4$:Yb,Er UCNPs. In this ligand oxidation process, the oleic acid capped on the surface of UCNPs was oxidized into azelaic acid, resulting in an extension of the newly generated free carboxylic groups (Figure 7c). They demonstrated that the oxidation did not affect the morphology, phase transition, composition, or UC fluorescence of the UCNPs. These modified UCNPs could be easily dispersed in water and further conjugated with biomolecules such as streptavidin due to the free carboxylic groups on the surface of the UCNPs. However, this method is only applicable to a specific class of UCNPs such as those capped with a ligand containing an unsaturated carbon-carbon bond in its long alkyl chain.

Wang *et al.*[109] used a more applicable method, layer-by-layer (LbL) assembly to convert the hydrophobic UCNPs into hydrophilic. This method involved electrostatic attractions between the oppositely charged species deposited. At weakly basic conditions (pH 8.5), the UCNPs were negatively charged and fabricated using positively charged polyallylamine hydrochloride (PAH), giving positively charged NPs. Subsequently, negatively charged polystyrene sulfonate (PSS) was used to assemble the resultant NPs which was then assembled by PAH again (Figure 7d). After the LbL assembly process, amino groups from the amino-rich PAH were introduced onto the surface of the UCNPs, allowing the modified NPs to be attached to biomolecules such as biotin. The advantage of the LbL assembly method is that it permits the preparation of coated colloids with varying shapes and sizes as well as precise control of the thickness layer of the polymer. However, before modification, the NPs are usually required to be hydrophilic.

5. Biological applications of RE doped $NaYF_4$ UCNPs

5.1. *In vitro* cellular imaging and *in vivo* tissue imaging

The excitation of RE doped UCNPs often requires IR radiation. The use of IR radiation has great advantages in cell and tissue imaging because they provide (i) a high signal-to-noise ratio, (ii) strong penetration ability (can penetrate tissues up to several inches) inherent to the long wavelength excitation light, and (iii) less photo damage to the cell/tissue under long-term irradiation.[110] Therefore, RE doped UCNPs are promising alternatives to traditional fluorescent biolabels (such as organic dyes and QDs) for *in vitro* cell and *in vivo* tissue imaging.

5.1.1. *In vitro* cell labeling and imaging—Three years ago, Chatterjee *et al.*[111] reported the first use of $NaYF_4$:Yb,Er UCNPs for cellular imaging in which the $NaYF_4$:Yb,Er UCNPs were first functionalized with PEI and later covalently conjugated with folic acid to form folic acid modified $NaYF_4$:Yb,Er UCNPs. The folic acid modified $NaYF_4$:Yb,Er UCNPs were then incubated with human HT29 adenocarcinoma cells and human OVCAR3 ovarian carcinoma cells under physiological conditions for 24 h. As a result of the abnormally high levels of folate receptors expressed on the surface of both cells, the folic acid modified UCNPs were able to specifically target the cells. As shown in Figure 8, when attached, the UCNPs could emit green UC fluorescence under a confocal microscope equipped with a 980 nm laser. Their control experiment demonstrated that the

binding between the folic acid modified UCNPs and the folic acid receptors expressed on the cell surface was target specific.

In the same year, Jalil et al.[112] reported the *in vitro* cytotoxic effect of silica coated NaYF$_4$:Yb,Er UCNPs on two types of cells: rat skeletal myoblasts and bone marrow-derived stem cells (BMSCs). In their studies, the silica coated NaYF$_4$:Yb,Er UCNPs excluding any functionalization, were incubated under physiological conditions with the two cell types for 24 h. As shown in Figure 9, observed using a confocal microscope under 980 nm radiation, the silica coated UCNPs were mainly located in the cytoplasmic and perinuclear regions shown by bright green fluorescence. They also demonstrated that both the rat skeletal myoblasts and BMSCs survived reasonably well even at relatively high concentrations of UCNPs (100 μg/ml in this study) indicating that the silica coated NaYF$_4$:Yb,Er UCNPs had good *in vitro* biocompatibility for cellular imaging.

Nyk et al.[113] reported high contrast imaging of human pancreatic cancer cells (Panc 1) using NaYF$_4$:Yb,Tm UCNPs. In their studies, OA coated NaYF$_4$:Yb,Tm UCNPs were first modified with 3-mercaptopropionic acid (MPA) to make them water-soluble and then incubated with Panc 1 cells at 37 °C for 2 h. Under a 980 nm excitation, the NPs on the surface of the cells could emit IR light at approximately 800 nm (Figure 10), when viewed under a Nuance GNIR CCD camera. It should be noted that the photoluminescence imaging showed high contrast, inherent three-dimensional localization features and a complete absence of autofluorescence. In addition, no overt toxicity of these UCNPs was found during the cell viability assay.

Our group, Wang et al.[114, 115] have recently reported an effective and time efficient method for immunolabelling and imaging of HeLa cells via silica coated NaYF$_4$:Yb,Er and NaYbF$_4$:Er/Tm/Ho UCNPs. In this study, the silica coated amino-modified UCNPs were first linked to the rabbit anti-CEA8 antibody to form antibody modified UCNPs and were then incubated with HeLa cells in physiological conditions for 1 h. During the incubation period, the immunoreaction between the rabbit anti-CEA8 antibody modified UCNPs and carcinoembryonic antigens (CEA) expressed on HeLa cell membranes occurred resulting in an attachment of the UCNPs to the surface of the cells (Figure 11a). As a result, HeLa cells were labeled by UCNPs. From the control experiments, we demonstrated that this immunolabelling exhibited high specificity (Figure 11b–d).

Jiang et al.[116] also used folic acid and anti-Her2 antibody conjugated NaYF$_4$:Yb,Er UCNPs for labeling and fluorescent imaging of HT-29 cells and SK-BR-3 cells, respectively. More interestingly, NaYF$_4$:Yb,Er UCNPs were used in this work for the delivery and tracking of siRNA (small interference RNA). The siRNA was first attached to anti-Her2 antibody conjugated UCNPs and then attached to SK-BR-3 cells via an immunoreaction between the anti-HER2 antibody and HER2 receptors of SK-BR-3 cells. This led to the delivery of siRNA to the SK-BR-3 cells. The intracellular delivery was tracked using a confocal laser scanning microscopy equipped with an NIR laser and the effect of siRNA on gene silencing was studied using a luciferase assay.

Shan et al.[117] reported the use of carboxyl functionalized NaYF$_4$:Yb,Er UCNPs for the imaging of AB12 mouse mesothelioma cells. From the TEM and fluorescent images, they concluded that these NaYF$_4$:Yb,Er UCNPs could enter into the cells indicating a high biocompatibility of the carboxyl functionalized NaYF$_4$:Yb,Er UCNPs. In addition, other kinds of UCNPs such as LaF$_3$:Yb,Ho NPs were also used as biological labels for cell imaging.[118]

Cytotoxicity tests can be used as an effective and sensitive way to assess the harmful components contained in UCNPs. The cytotoxicity of UCNPs to cells is often measured by

3-(4,5-dimethylthiazol-2-yl)-2,5-diphenyltetrazolium bromide (MTT) assays [111–113] or 3-(4,5-dimethylthiazol-2-yl)-5-(3-carboxymethoxyphenyl)-2-(4-sulfophenyl)-2H-tetrazoli um, innersalt (MTS) assays [116–119]. Typically, the UCNPs in various concentrations are incubated with cells for a period of incubation times, and then cell viability is scored under both control and exposed conditions to characterize the cytotoxic effect. Table 3 lists the data of cytotoxicity tests on UCNPs to different cells, which can prove that RE doped UCNPs exhibit low cytotoxicity and are even non-cytotoxic to a broad range of cells.

5.1.2. *In vivo* **tissue imaging**—Chatterjee *et al.*[111] first reported the *in vivo* imaging of deep tissues in the Wistar rat using UCNPs. In their studies, PEI (5 wt%) was used for the coating of NaYF$_4$:Yb,Er UCNPs, and then 100 µl of resultant UCNPs (4.4 mg/ml) were injected subcutaneously into the groin and upper leg regions of the rat with a depth up to 10 mm. The rat was then excited using a 980 nm laser. As a result, the UCNPs injected below the abdominal skin, thigh muscles, and skin showed visible fluorescence under a 980 nm excitation. However, when the QDs (used as a control) were injected into the thicker skin or abdomen, they did not show any fluorescence under a UV excitation. Only QDs injected into the translucent skin of the foot could emit fluorescence (Figure 12a–f). Therefore, the NIR radiation proved to have better penetration ability than the UV light. UCNPs excited with NIR radiation therefore have great potential for *in vivo* imaging. Later, Nyk *et al.*[113] reported high contrast whole-body *in vivo* imaging of the Balb-c mouse injected with NaYF$_4$:Yb,Tm UCNPs (Figure 12g–h). They demonstrated that the UCNPs showed no significant toxicity in the mice after 48 h post injection. Their study provided a foundation for the development of 3-D imaging systems for advanced whole body optical imaging. However, from available literature, the use of UCNPs for *in vivo* imaging is still in its preliminary stages.[120, 121]

5.2. Biological detection and analysis

5.2.1. Detection based on fluorescence resonance energy transfer—
Fluorescence resonance energy transfer (FRET) is a nonradiative process where the electron excitation energy of a donor chromophore is transferred to a nearby acceptor molecule via long-range dipole-dipole interactions. In recent years, FRET-based analytical methods have gained considerable attention as powerful tools for biological detections because of their easy handling and high sensitivity.

To the best of our knowledge, the first demonstration of a FRET-based biological detection using NaYF$_4$:Yb,Er UCNPs was reported by Wang *et al.*.[109] In the FRET system, the amino-functionalized NaYF$_4$: Yb,Er UCNPs were conjugated with biotin to serve as the donor and the biotin modified Au NPs acted as the acceptor. When avidin was added into the system, a reaction between the biotin and avidin occurred where the distance between the donor and the acceptor was shortened and energy emitted from the donor was transferred to the acceptor effectively. The more avidin that was added, the more energy could be transferred to the Au NPs. Thus, a linear relationship between the relative fluorescence intensity and the concentration of avidin in the FRET system was established (Figure 13a). Using this method, trace amounts of avidin in the concentration range from 0.5 to 370 nM could be detected.

Chen *et al.* utilized NaYF$_4$:Yb,Er UCNPs to demonstrate their possible applications in the FRET system.[108] In their studies, carboxyl functionalized NaYF$_4$:Yb,Er UCNPs were covalently linked with streptavidin and then conjugated with biotin labeled DNA (capture-DNA). The resulting UCNPs were modified with capture-DNA which served as the donor, and TAMRA labeled reporter-DNA which could emit red light at the excitation of green light which acted as the acceptor (Figure 13b). When target-DNA was added into the

system, a sandwich-type hybridization occurred where two shorter DNA (capture-DNA and reporter-DNA) were captured by a longer DNA (target-DNA). The energy could then be effectively transferred from the UCNPs to TAMRA, enabling TAMRA to emit red light due to the shortened distance between the UCNPs and TAMRA. With an increasing concentration of target-DNA added into the system, the green emission at 540 nm measured from the UCNPs gradually decreased while the yellow emission at 580 nm from TAMRA was enhanced. In addition, the fluorescent intensity ratio (I_{580}/I_{540}) varied linearly with the concentration of target-DNA in the range of 10–50 nM.

Our group, Wang et al.[122] have also recently developed a luminescence resonance energy transfer (LRET)-based immunoassay. In this approach, amino-functionalized $NaYF_4$:Yb,Er UCNPs acted as a source for energy donor efficiency while gold NPs acted as an energy acceptor by absorbing the energy released by the donor molecules (Figure 14). This new sandwich based immunoassay system can be efficiently used for the detection of trace amounts of goat anti-human antibodies in the mg/ml range.

The above examples are significant contributions as they provide good models for FRET-based biological detections using RE doped UCNPs and can be used in the detection of other kinds of biomolecules such as antibodies.

5.2.2. Detection based on magnetic separation—Wang et al.[123] applied $NaYF_4$:Yb,Er UCNPs for the sensitive detection of trace amounts of DNA with the aid of magnetic bioseparation and concentration technology. First, the Fe_3O_4 magnetic NPs were covalently linked to capture-DNA and $NaYF_4$:Yb,Er UCNPs were conjugated with probe-DNA. As in a typical sandwich-type assay, the short capture-DNA on the surface of magnetic NPs was first hybridized with long target-DNA. Then the overhanging region of target-DNA was matched to UCNPs labeled with probe-DNA. As a result, the UCNPs were captured by the magnetic NPs through hybridization of the oligonucleotides and then purified by magnetic separation (Figure 15). The UC fluorescence intensity of the captured UCNPs was found to have a linear relationship with the concentration of target DNA in the range of 7.8–78.0 nM. This method detects trace amounts of DNA and is a good alternative to PCR. This magnetic separation and concentration technology may serve as a useful model for the development of bioanalytical devices for biodetections in the near future.

6. Summary and Future Outlook

This review is focused on the synthesis of RE doped $NaYF_4$ using various methodologies and summarizes the general synthetic strategies, surface modifications and biological applications of emerging next generation luminescent UCNPs. Even though, the UC luminescence phenomenon of RE doped nanomaterials was observed several years ago, only recently are its practical applications greatly realized. Owing to their unique luminescent properties, UCNPs are currently evolved as an alternative source to traditional fluorescent probes by overcoming their current limitations. These UCNPs offer a wide range of biomedical applications including *in vitro* labeling, imaging, and analysis including the detection based on FRET and magnetic separation. In the future these UCNPs applications are expected to find more applications in *in* vivo biomedical studies. Despite the significant advancement in developing different strategies to synthesize and modify UC nanomaterials, till date it lacks a generalized protocol for synthesizing ultra-small NPs with strong UC luminescence intensity for biomedical applications. Current studies confirm that UCNPs can provide an excellent platform for *in* vitro based optical imaging; however, more detailed studies are necessary in the future to prove its wide applicability in animal models. There is also a greater scope to develop biocompatible multifunctional UC nanomaterials with high photoluminescence ability, strong superparamagnetism and easy bioconjugation for

magnetic separation purposes in the coming years. Likewise, more focus is needed to develop new strategies for synthesizing UCNPs that can be extended to a variety of substrates for generating multiplexed detection devices.

Acknowledgments

References

1. Rao JH, Dragulescu-Andrasi A, Yao HQ. Fluorescence imaging in vivo: recent advances. Curr Opin Biotechnol. 2007; 18:17–25. [PubMed: 17234399]

2. Gao XH, Yang L, Petros JA, Marshall FF, Simons JW, Nie SM. In vivo molecular and cellular imaging with quantum dots. Curr Opin Biotechnol. 2005; 16:63–72. [PubMed: 15722017]

3. Shen J, Sun LD, Yan CH. Luminescent rare earth nanomaterials for bioprobe applications. Dalton Trans. 2008; 42:5687–97. [PubMed: 18941653]

4. Jamieson T, Bakhshi R, Petrova D, Pocock R, Imani M, Seifalian AM. Biological applications of quantum dots. Biomaterials. 2007; 28:4717–32. [PubMed: 17686516]

5. Wang X, Li YD. Monodisperse nanocrystals: general synthesis, assembly, and their applications. Chem Commun. 2007; 28:2901–10.

6. Smith AM, Gao XH, Nie SM. Quantum dot nanocrystals for in vivo molecular and cellular imaging. Photochem Photobiol. 2004; 80:377–85. [PubMed: 15623319]

7. Chan WCW, Nie SM. Quantum dot bioconjugates for ultrasensitive nonisotopic detection. Science. 1998; 281:2016–8. [PubMed: 9748158]

8. Smith AM, Duan HW, Mohs AM, Nie SM. Bioconjugated quantum dots for in vivo molecular and cellular imaging. Adv Drug Deliv Rev. 2008; 60:1226–40. [PubMed: 18495291]

9. Chang E, Thekkek N, Yu WW, Colvin VL, Drezek R. Evaluation of quantum dot cytotoxicity based on intracellular uptake. Small. 2006; 2:1412–7. [PubMed: 17192996]

10. Auzel F. Upconversion and anti-stokes processes with f and d ions in solids. Chem Rev. 2004; 104:139–73. [PubMed: 14719973]

11. Wang F, Liu XG. Recent advances in the chemistry of lanthanide-doped upconversion nanocrystals. Chem Soc Rev. 2009; 38:976–89. [PubMed: 19421576]

12. Vetrone F, Capobianco JA. Lanthanide-doped fluoride nanoparticles: luminescence, upconversion, and biological applications. Int J Nanotechnol. 2008; 5:1306–39.

13. Wang F, Banerjee D, Liu YS, Chen XY, Liu XG. Upconversion nanoparticles in biological labeling, imaging, and therapy. Analyst. 2010; 135:1839–54. [PubMed: 20485777]

14. Li CX, Lin J. Rare earth fluoride nano-/microcrystals: synthesis, surface modification and application. J Mater Chem. 2010; 20:6821–47.

15. Bunzli Jean-Claude G. Lanthanide luminescence for biomedical analyses and imaging. Chem Rev. 2010; 110:2729–55. [PubMed: 20151630]

16. Joubert MF. Photon avalanche upconversion in rare earth laser materials. Opt Mater. 1999; 11:181–203.

17. Bloembergen N. Solid state infrared quantum counters. Phys Rev Lett. 1959; 2:84–5.

18. Auzel FE. Materials and devices using double-pumped phosphors with energy transfer. Proc IEEE. 1973; 61:758–86.

19. Chivian JS, Case WE, Eden DD. The photon avalanche: a new phenomenon in Pr^{3+}-based infrared quantum counters. Phys Rev Lett. 1979; 35:124–125.

20. Vetrone F, Boyer JC, Capobianco JA, Speghini A, Bettinelli M. Significance of Yb^{3+} concentration on the upconversion mechanismsin codoped $Y_2O_3:Er^{3+},Yb^{3+}$ nanocrystals. J Appl Phys. 2004; 96:661–7.

21. Xue N, Fan XP, Wang ZY, Wang MQ. Synthesis process and luminescence properties of Ln^{3+} doped $NaY(WO_4)_2$ nanoparticles. Mater Lett. 2007; 61:1576–9.

22. Matsuura D. Red, green, and blue upconversion luminescence of trivalent-rare-earth ion-doped Y_2O_3 nanocrystals. Appl Phys Lett. 2002; 81:4526–8.

23. Su J, Song F, Tan H, Han L, Zhou F, Tian JG, et al. Phonon-assisted mechanisms and concentration dependence of Tm^{3+} blue upconversion luminescence in codoped $NaY(WO_4)_2$ crystals. J Phys D: Appl Phys. 2006; 39:2094–9.

24. Yang LM, Song HW, Yu LX, Liu ZX, Lu SH. Unusual power-dependent and time-dependent upconversion luminescence in nanocrystals $Y_2O_3:Ho^{3+}/Yb^{3+}$ J Lumin. 2006; 116:101–6.

25. Yang J, Zhang CM, Peng C, Li CX, Wang LL, Chai RT, et al. Controllable red, green, blue (RGB) and bright white upconversion luminescence of $Lu_2O_3:Yb^{3+}/Er^{3+}/Tm^{3+}$ nanocrystals through single laser excitation at 980 nm. Chem Eur J. 2009; 15:4649–55. [PubMed: 19296483]

26. Pandozzi F, Vetrone F, Boyer JC, Naccache R, Capobianco JA, Speghini A, et al. A spectroscopic analysis of blue and ultraviolet upconverted emissions from $Gd_3Ga_5O_{12}:Tm^{3+},Yb^{3+}$ nanocrystals. J Phys Chem B. 2005; 109:17400–5. [PubMed: 16853224]

27. Liu HQ, Wang LL, Chen SG. Effect of Yb^{3+} concentration on the upconversion of Er^{3+} ion doped La_2O_3 nanocrystals under 980 nm excitation. Mater Lett. 2007; 61:3629–31.

28. Tsuboi T. Upconversion emission in Er^{3+}/Yb^{3+}-codoped YVO_4 crystals. Phys Rev B. 2000; 62:4200–3.

29. Singh S, Kumar K, Rai SB. Multifunctional Er^{3+}-Yb^{3+} codoped Gd_2O_3 nanocrystalline phosphor synthesized through optimized combustion route. Appl Phys B. 2009; 94:165–73.

30. Yi GS, Chow GM. Colloidal $LaF_3:Yb,Er$, $LaF_3:Yb,Ho$ and $LaF_3:Yb,Tm$ nanocrystals with multicolor upconversion fluorescence. J Mater Chem. 2005; 15:4460–4.

31. Pires AM, Serra OA, Davolos MR. Yttrium oxysulfide nanosized spherical particles doped with Yb and Er or Yb and Tm: efficient materials for up-converting phosphor technology field. J Alloy Compd. 2004; 374:181–4.

32. Liu CH, Chen DP. Controlled synthesis of hexagon shaped lanthanide-doped LaF_3 nanoplates with multicolor upconversion fluorescence. J Mater Chem. 2007; 17:3875–80.

33. Hu H, Chen ZG, Cao TY, Zhang Q, Yu MX, Li FY, et al. Hydrothermal synthesis of hexagonal lanthanide-doped LaF_3 nanoplates with bright upconversion luminescence. Nanotechnology. 2008; 37:375702. [PubMed: 21832556]

34. Hirai T, Orikoshi T. Preparation of $Gd_2O_3:Yb,Er$ and $Gd_2O_2S:Yb,Er$ infrared-to-visible conversion phosphor ultrafine particles using an emulsion liquid membrane system. J Colloid Interf Sci. 2004; 269:103–8.

35. Yan RX, Li YD. Down/up conversion in Ln^{3+}-doped YF_3 nanocrystals. Adv Funct Mater. 2005; 15:763–70.

36. Luo XX, Cao WH. Ethanol-assistant solution combustion method to prepare $La_2O_2S:Yb,Pr$ nanometer phosphor. J Alloys Compd. 2008; 460:529–34.

37. Wang GF, Qin WP, Zhang JS, Wang Y, Cao CY, Wang LL, et al. Synthesis, growth mechanism, and tunable upconversion luminescence of Yb^{3+}/Tm^{3+}-codoped YF_3 nanobundles. J Phys Chem C. 2008; 112:12161–7.

38. Xiao SG, Yang XL, Ding JW, Yan XH. Up-conversion in Yb^{3+}-Tm^{3+} co-doped lutetium fluoride particles prepared by a combustion-fluorization method. J Phys Chem C. 2007; 111:8161–5.

39. Du YP, Zhang YW, Sun LD, Yan CH. Luminescent monodisperse nanocrystals of lanthanide oxyfluorides synthesized from trifluoroacetate precursors in high-boiling solvents. J Phys Chem C. 2008; 112:405–15.

40. Gao L, Ge X, Chai ZL, Xu GH, Wang X, Wang C. Shape-controlled synthesis of octahedral α-$NaYF_4$ and its rare earth doped submicrometer particles in acetic acid. Nano Res. 2009; 2:565–74.

41. Li ZH, Zheng LZ, Zhang LN, Xiong LY. Synthesis, characterization and upconversion emission properties of the nanocrystals of Yb^{3+}/Er^{3+}-codoped YF_3-YOF-Y_2O_3 system. J Lumin. 2007; 126:481–6.

42. Wang M, Liu JL, Zhang YX, Hou W, Wu XL, Xu SK. Two-phase solvothermal synthesis of rare-earth doped $NaYF_4$ upconversion fluorescent nanocrystals. Mater Lett. 2009; 63:325–7.

43. Lisiecki R, Ryba-Romanowski W, Speghini A, Bettinelli M. Luminescence spectroscopy of Er^{3+}-doped and Er^{3+}, Yb^{3+}-codoped $LaPO_4$ single crystals. J Lumin. 2009; 129:521–5.

44. Pei XJ, Hou YB, Zhao SL, Xu Z, Teng F. Frequency upconversion of Tm^{3+} and Yb^{3+} codoped $YLiF_4$ synthesized by hydrothermal method. Mater Chem Phys. 2005; 90:270–4.

45. Heer S, Lehmann O, Haase M, Gudel HU. Blue, green, and red upconversion emission from lanthanide-doped $LuPO_4$ and $YbPO_4$ nanocrystals in a transparent colloidal solution. Angew Chem Int Ed. 2003; 42:3179–82.

46. Naccache R, Vetrone F, Mahalingam V, Cuccia LA, Capobianco JA. Controlled synthesis and water dispersibility of hexagonal phase $NaGdF_4$:Ho^{3+}/Yb^{3+} nanoparticles. Chem Mater. 2009; 21:717–23.

47. Mahalingam V, Vetrone F, Naccache R, Speghini A, Capobianco JA. Structural and optical investigation of colloidal Ln^{3+}/Yb^{3+} co-doped KY_3F_{10} nanocrystals. J Mater Chem. 2009; 19:3149–52.

48. Yi GS, Sun BQ, Yang FZ, Chen DP, Zhou YX, Cheng J. Synthesis and characterization of high-efficiency nanocrystal up-conversion phosphors: ytterbium and erbium codoped lanthanum molybdate. Chem Mater. 2002; 14:2910–4.

49. Liang LF, Zhang XM, Hu HL, Feng L, Wu MM, Su Q. Up-conversion properties in KGd_2F_7:Yb^{3+}/Er^{3+} Mater Lett. 2005; 59:2186–90.

50. Chen ZX, Bu WB, Zhang N, Shi JL. Controlled construction of monodisperse $La_2(MoO_4)_3$:Yb,Tm microarchitectures with upconversion luminescent property. J Phys Chem C. 2008; 112:4378–83.

51. Vetrone F, Mahalingam V, Capobianco JA. Near-infrared-to-blue upconversion in colloidal $BaYF_5$:Tm^{3+},Yb^{3+} nanocrystals. Chem Mater. 2009; 21:1847–51.

52. Page RH, Schaffers KI, Waide PA, Tassano JB, Payne SA, Krupke WF, et al. Upconversion-pumped luminescence efficiency of rare-earth-doped hosts sensitized with trivalent ytterbium. J Opt Soc Am B. 1998; 15:996–1008.

53. Wang F, Han Y, Lim CS, Lu YH, Wang J, Xu J, et al. Simultaneous phase and size control of upconversion nanocrystals through lanthanide doping. Nature. 2010; 463:1061–5. [PubMed: 20182508]

54. Thoma RE, Insley H, Hebert GM. The sodium fluoride-lanthanide trifluoride systems. Inorg Chem. 1966; 5:1222–9.

55. Mai HX, Zhang YW, Si R, Yan ZG, Sun LD, You LP, et al. High-quality sodium rare-earth fluoride nanocrystals: controlled synthesis and optical properties. J Am Chem Soc. 2006; 128:6426–36. [PubMed: 16683808]

56. Yi GS, Lu HC, Zhao SY, Yue G, Yang WJ, Chen DP, et al. Synthesis, characterization, and biological application of size-controlled nanocrystalline $NaYF_4$:Yb,Er infrared-to-visible up-conversion phosphors. Nano Lett. 2004; 4:2191–6.

57. Wei Y, Lu FQ, Zhang XR, Chen DP. Synthesis and characterization of efficient near-infrared upconversion Yb and Tm codoped $NaYF_4$ nanocrystal reporter. J Alloys Compd. 2007; 427:333–40.

58. Zhang YW, Sun X, Si R, You LP, Yan CH. Single-crystalline and monodisperse LaF_3 triangular nanoplates from a single-source precursor. J Am Chem Soc. 2005; 127:3260–1. [PubMed: 15755126]

59. Boyer JC, Vetrone F, Cuccia LA, Capobianco JA. Synthesis of colloidal upconverting NaYF$_4$ nanocrystals doped with Er^{3+}, Yb^{3+} and Tm^{3+}, Yb^{3+} via thermal decomposition of lanthanide trifluoroacetate precursors. J Am Chem Soc. 2006; 128:7444–5. [PubMed: 16756290]

60. Boyer JC, Cuccia LA, Capobianco JA. Synthesis of colloidal upconverting NaYF$_4$:Er^{3+}/Yb^{3+} and Tm^{3+}/Yb^{3+} monodisperse nanocrystals. Nano Lett. 2007; 7:847–52. [PubMed: 17302461]

61. Mai HX, Zhang YW, Sun LD, Yan CH. Size- and phase-controlled synthesis of monodisperse NaYF$_4$:Yb,Er nanocrystals from a unique delayed nucleation pathway monitored with upconversion spectroscopy. J Phys Chem C. 2007; 111:13730–9.

62. Ehlert O, Thomann R, Darbandi M, Nann T. A four-color colloidal multiplexing nanoparticle system. ACS Nano. 2008; 2:120–4. [PubMed: 19206555]

63. Du YP, Zhang YW, Yan ZG, Sun LD, Gao S, Yan CH. Single-crystalline and near-monodispersed NaMF$_3$ (M = Mn, Co, Ni, Mg) and LiMAlF$_6$ (M = Ca, Sr) nanocrystals from cothermolysis of multiple trifluoroacetates in solution. Chem Asian J. 2007; 2:965–74. [PubMed: 17534994]

64. Shan JN, Qin X, Yao N, Ju YG. Synthesis of monodisperse hexagonal NaYF$_4$:Yb,Ln (Ln = Er, Ho and Tm) upconversion nanocrystals in TOPO. Nanotechnology. 2007; 18:1–7.

65. Shan JN, Ju YG. A single-step synthesis and the kinetic mechanism for monodisperse and hexagonal-phase NaYF$_4$:Yb,Er upconversion nanophosphors. Nanotechnolog. 2009; 20:275603.

66. Wei Y, Lu FQ, Zhang XR, Chen DP. Synthesis of oil-dispersible hexagonal-phase and hexagonal-shaped NaYF$_4$:Yb,Er nanoplates. Chem Mater. 2006; 18:5733–7.

67. Sun YJ, Chen Y, Tian LJ, Yu Y, Kong XG, Zhao JW, et al. Controlled synthesis and morphology dependent upconversion luminescence of NaYF$_4$:Yb,Er nanocrystals. Nanotechnology. 2007; 18:275609.

68. Li CX, Quan ZW, Yang J, Yang PP, Lin J. Highly uniform and monodisperse α-NaYF$_4$:Ln^{3+} (Ln = Eu, Tb, Yb/Er, and Yb/Tm) hexagonal microprism crystals: hydrothermal synthesis and luminescent properties. Inorg Chem. 2007; 46:6329–37. [PubMed: 17602610]

69. Zhuang JL, Liang LF, Sung HHY, Yang XF, Wu MM, Williams ID, et al. Controlled hydrothermal growth and up-conversion emission of NaLnF$_4$ (Ln = Y, Dy-Yb). Inorg Chem. 2007; 46:5405–10.

70. Li CX, Zhang CM, Hou ZY, Wang LL, Quan ZW, Lian HZ, et al. β-NaYF$_4$ and β-NaYF$_4$:Eu^{3+} microstructures: morphology control and tunable luminescence properties. J Phys Chem C. 2009; 113:2332–9.

71. Li CX, Yang J, Quan ZW, Yang PP, Kong DY, Lin J. Different microstructures of β-NaYF$_4$ fabricated by hydrothermal process: Effects of pH values and fluoride sources. Chem Mater. 2007; 19:4933–42.

72. Li CX, Quan ZW, Yang PP, Yang J, Lian HZ, Lin J. Shape controllable synthesis and upconversion properties of NaYbF$_4$/NaYbF$_4$:Er^{3+} and YbF$_3$/YbF$_3$:Er^{3+} microstructures. J Mater Chem. 2008; 18:1353–61.

73. Wang ZJ, Tao F, Yao LZ, Cai WL, Li XG. Selected synthesis of cubic and hexagonal NaYF$_4$ crystals via a complex-assisted hydrothermal route. J Cryst Growth. 2006; 290:296–300.

74. Wang ZJ, Tao F, Cai WL, Yao LZ, Li XG. Controlled-synthesis and up-conversion luminescence of NaYF$_4$:Yb,Er phosphors. Solid State Commun. 2007; 144:255–8.

75. Liang X, Wang X, Zhuang J, Peng Q, Li YD. Branched NaYF$_4$ nanocrystals with luminescent properties. Inorg Chem. 2007; 46:6050–5. [PubMed: 17602472]

76. Zeng JH, Su J, Li ZH, Yan RX, Li YD. Synthesis and upconversion luminescence of hexagonal-phase NaYF$_4$:Yb, Er phosphors of controlled size and morphology. Adv Mater. 2005; 17:2119–23.

77. Zeng JH, Li ZH, Su J, Wang LY, Yan RX, Li YD. Synthesis of complex rare earth fluoride nanocrystal phosphors. Nanotechnology. 2006; 17:3549–55. [PubMed: 19661603]

78. Wang F, Chatterjee DK, Li ZQ, Zhang Y, Fan XP, Wang MQ. Synthesis of polyethylenimine/NaYF$_4$ nanoparticles with upconversion fluorescence. Nanotechnology. 2006; 17:5786–91.

79. Wang F, Liu XG. Upconversion multicolor fine-tuning: visible to near-infrared emission from lanthanide-doped NaYF$_4$ nanoparticles. J Am Chem Soc. 2008; 130:5642–3. [PubMed: 18393419]

80. Wang X, Zhuang J, Peng Q, Li YD. A general strategy for nanocrystal synthesis. Nature. 2005; 437:121–4. [PubMed: 16136139]

81. Liang X, Wang X, Zhuang J, Peng Q, Li YD. Synthesis of NaYF$_4$ nanocrystals with predictable phase and shape. Adv Funct Mater. 2007; 17:2757–65.

82. Wang LY, Li YD. Na(Y$_{1.5}$Na$_{0.5}$)F$_6$ Single-crystal nanorods as multicolor luminescent materials. Nano Lett. 2006; 6:1645–9. [PubMed: 16895350]

83. Wang LY, Li YD. Controlled synthesis and luminescence of lanthanide doped NaYF$_4$ nanocrystals. Chem Mater. 2007; 19:727–34.

84. Wang M, Mi CC, Liu JL, Wu XL, Zhang YX, Hou W, et al. One-step synthesis and characterization of water-soluble NaYF$_4$:Yb,Er/polymer nanoparticles with efficient up-conversion fluorescence. J Alloys Compd. 2009; 485:24–7.

85. Chen X, Wang WJ, Chen XY, Bi JH, Wu L, Li ZH, et al. Microwave hydrothermal synthesis and upconversion properties of NaYF$_4$:Yb^{3+},Tm^{3+} with microtube morphology. Mater Lett. 2009; 63:1023–6.

86. Zhao JW, Sun YJ, Kong XG, Tian LJ, Wang Y, Tu LP, et al. Controlled synthesis, formation mechanism, and great enhancement of red upconversion luminescence of NaYF$_4$:Yb^{3+},Er^{3+} nanocrystals/submicroplates at low doping level. J Phys Chem B. 2008; 112:15666–72. [PubMed: 19367869]

87. Chen JY, Herricks T, Xia YN. Polyol synthesis of platinum nanostructures: Control of morphology through the manipulation of reduction kinetics. Angew Chem Int Ed. 2005; 44:2589–92.

88. Feldmann C, Jungk HO. Polyol-mediated preparation of nanoscale oxide particles. Angew Chem Int Ed. 2001; 40:359–62.

89. Feldmann C, Jungk HO. Preparation of sub-micrometer LnPO$_4$ particles (Ln = La, Ce). J Mater Sci. 2002; 37:3251–4.

90. Wei Y, Lu FQ, Zhang XR, Chen DP. Polyol-mediated synthesis and luminescence of lanthanide-doped NaYF$_4$ nanocrystal upconversion phosphors. J Alloys Compd. 2008; 455:376–84.

91. Qin RF, Song HW, Pan GH, Hu LY, Yu HQ, Li SW, et al. Polyol-mediated syntheses and characterizations of NaYF$_4$, NH$_4$Y$_3$F$_{10}$ and YF$_3$ nanocrystals/sub-microcrystals. Mater Res Bull. 2008; 43:2130–6.

92. Li ZQ, Zhang Y. An efficient and user-friendly method for the synthesis of hexagonal-phase NaYF$_4$:Yb,Er/Tm nanocrystals with controllable shape and upconversion fluorescence. Nanotechnology. 2008; 19:345606. [PubMed: 21730655]

93. Heer S, Kompe K, Gudel HU, Haase M. Highly efficient multicolour upconversion emission in transparent colloids of lanthanide-doped NaYF$_4$ nanocrystals. Adv Mater. 2004; 16:2102–5.

94. Wang L, Zhao WJ, Tan WH. Bioconjugated silica nanoparticles: development and applications. Nano Res. 2008; 1:99–115.

95. Li ZQ, Zhang Y. Monodisperse silica-coated polyvinylpyrrolidone/NaYF$_4$ nanocrystals with multicolor upconversion fluorescence emission. Angew Chem Int Ed. 2006; 45:7732–5.

96. Shan JN, Ju YG. Controlled synthesis of lanthanide-doped NaYF$_4$ upconversion nanocrystals via ligand induced crystal phase transition and silica coating. Appl Phys Lett. 2007; 91:123101–3.

97. Johnson NJJ, Sangeetha NM, Boyer JC, van Veggel FCJM. Facile ligand-exchange with polyvinylpyrrolidone and subsequent silica coating of hydrophobic upconverting β-NaYF$_4$:Yb^{3+}/Er^{3+} nanoparticles. Nanoscale. 2010; 2:771–7. [PubMed: 20648323]

98. Li ZQ, Zhang Y, Jiang S. Multicolor core/shell-structured upconversion fluorescent nanoparticles. Adv Mater. 2008; 20:4765–9.

99. Zhang MF, Shi SJ, Meng JX, Wang XQ, Fan H, Zhu YC, et al. Preparation and characterization of near-infrared luminescent biofunctional core/shell nanocomposites. J Phys Chem C. 2008; 112:2825–30.

100. Lu HC, Yi GS, Zhao SY, Chen DP, Guo LH, Cheng J. Synthesis and characterization of multi-functional nanoparticles possessing magnetic, up-conversion fluorescence and bio-affinity properties. J Mater Chem. 2004; 14:1336–41.

101. Liu ZY, Yi GS, Zhang HT, Ding J, Zhang YW, Xue JM. Monodisperse silica nanoparticles encapsulating upconversion fluorescent and superparamagnetic nanocrystals. Chem Commun. 2008; 29:694–6.

102. Mi CC, Zhang JP, Gao HY, Wu XL, Wang M, Wu YF, et al. Multifunctional nanocomposites of superparamagnetic (Fe$_3$O$_4$) and NIR-responsive rare earth-doped up-conversion fluorescent

(NaYF$_4$:Yb,Er) nanoparticles and their applications in biolabeling and fluorescent imaging of cancer cells. Nanoscale. 2010; 2:1141–8. [PubMed: 20648340]

103. Schafer H, Ptacek P, Kompe K, Haase M. Lanthanide-doped NaYF$_4$ nanocrystals in aqueous solution displaying strong up-conversion emission. Chem Mater. 2007; 19:1396–400.

104. Yi GS, Chow GM. Synthesis of hexagonal-phase NaYF$_4$:Yb,Er and NaYF$_4$:Yb,Tm nanocrystals with efficient up-conversion fluorescence. Adv Funct Mater. 2006; 16:2324–9.

105. Zhang QB, Song K, Zhao JW, Kong XG, Sun YJ, Liu XM, et al. Hexanedioic acid mediated surface-ligand-exchange process for transferring NaYF$_4$:Yb/Er (or Yb/Tm) up-converting nanoparticles from hydrophobic to hydrophilic. J Colloid Interf Sci. 2009; 336:171–5.

106. Boyer JC, Manseau MP, Murray JI, van Veggel FCJM. Surface modification of upconverting NaYF$_4$ nanoparticles with PEG-phosphate ligands for NIR (800 nm) biolabeling within the biological window. Langmuir. 2010; 26:1157–64. [PubMed: 19810725]

107. Yi GS, Chow GM. Water-soluble NaYF$_4$:Yb, Er(Tm)/NaYF$_4$/polymer core/shell/shell nanoparticles with significant enhancement of upconversion fluorescence. Chem Mater. 2007; 19:341–3.

108. Chen ZG, Chen HL, Hu H, Yu MX, Li FY, Zhang Q, et al. Versatile synthesis strategy for carboxylic acid-functionalized upconverting nanophosphors as biological labels. J Am Chem Soc. 2008; 130:3023–9. [PubMed: 18278910]

109. Wang LY, Yan RX, Huo ZY, Wang L, Zeng JH, Bao J, et al. Fluorescence resonant energy transfer biosensor based on upconversion luminescent nanoparticles. Angew Chem Int Ed. 2005; 44:6054–7.

110. Sivakumar S, Diamente PR, van Veggel FCJM. Silica-coated Ln^{3+}-doped LaF$_3$ nanoparticles as robust down- and upconverting biolabels. Chem Eur J. 2006; 12:5878–84. [PubMed: 16741910]

111. Chatterjee DK, Rufaihah AJ, Zhang Y. Upconversion fluorescence imaging of cells and small animals using lanthanide doped nanocrystals. Biomaterials. 2008; 29:937–43. [PubMed: 18061257]

112. Jalil RA, Zhang Y. Biocompatibility of silica coated NaYF$_4$ upconversion fluorescent nanocrystals. Biomaterials. 2008; 29:4122–8. [PubMed: 18675453]

113. Nyk M, Kumar R, Ohulchanskyy TY, Bergey EJ, Prasad PN. High contrast in vitro and in vivo photoluminescence bioimaging using near infrared to near infrared up-conversion in Tm^{3+} and Yb^{3+} doped fluoride nanophosphors. Nano Lett. 2008; 8:3834–8. [PubMed: 18928324]

114. Wang M, Mi CC, Wang WX, Liu CH, Wu YF, Xu ZR, et al. Immunolabeling and NIR-excited fluorescent imaging of HeLa cells by using NaYF$_4$:Yb,Er upconversion nanoparticles. ACS Nano. 2009; 3:1580–6. [PubMed: 19476317]

115. Wang M, Mi CC, Zhang YX, Liu JL, Li F, Mao CB, et al. NIR-responsive silica-coated NaYbF$_4$:Er/Tm/Ho upconversion fluorescent nanoparticles with tunable emission colors and their applications in immunolabeling and fluorescent imaging of cancer cells. J Phys Chem C. 2009; 113:19021–7.

116. Jiang S, Zhang Y, Lim KM, Sim EKW, Ye L. NIR-to-visible upconversion nanoparticles for fluorescent labeling and targeted delivery of siRNA. Nanotechnology. 2009; 20:155101. [PubMed: 19420539]

117. Shan JN, Chen JB, Meng J, Collins J, Soboyejo W, Friedberg JS, et al. Biofunctionalization, cytotoxicity, and cell uptake of lanthanide doped hydrophobically ligated NaYF$_4$ upconversion nanophosphors. J Appl Phys. 2008; 104:094308.

118. Hu H, Yu MX, Li FY, Chen ZG, Gao X, Xiong LQ, et al. Facile epoxidation strategy for producing amphiphilic up-converting rare-earth nanophosphors as biological labels. Chem Mater. 2008; 20:7003–9.

119. Xiong LQ, Yang TS, Yang Y, Xu CJ, Li FY. Long-term in vivo biodistribution imaging and toxicity of polyacrylic acid-coated upconversion nanophosphors. Biomaterials. 2010; 31:7078–85. [PubMed: 20619791]

120. Lim SF, Riehn R, Ryu WS, Khanarian N, Tung CK, Tank D, et al. In vivo and scanning electron microscopy imaging of upconverting nanophosphors in caenorhabditis elegans. Nano Lett. 2006; 6:169–74. [PubMed: 16464029]

121. Hilderbrand SA, Shao FW, Salthouse C, Mahmood U, Weissleder R. Upconverting luminescent nanomaterials: application to in vivo bioimaging. Chem Commun. 2009; 28:4188–90.

122. Wang M, Hou W, Mi CC, Wang WX, Xu ZR, Teng HH, et al. Immunoassay of goat antihuman immunoglobulin G antibody based on luminescence resonance energy transfer between near-infrared responsive NaYF$_4$:Yb, Er upconversion fluorescent nanoparticles and gold nanoparticles. Anal Chem. 2009; 81:8783–9. [PubMed: 19807113]

123. Wang LY, Li YD. Green upconversion nanocrystals for DNA detection. Chem Commun. 2006; 24:2557–9.
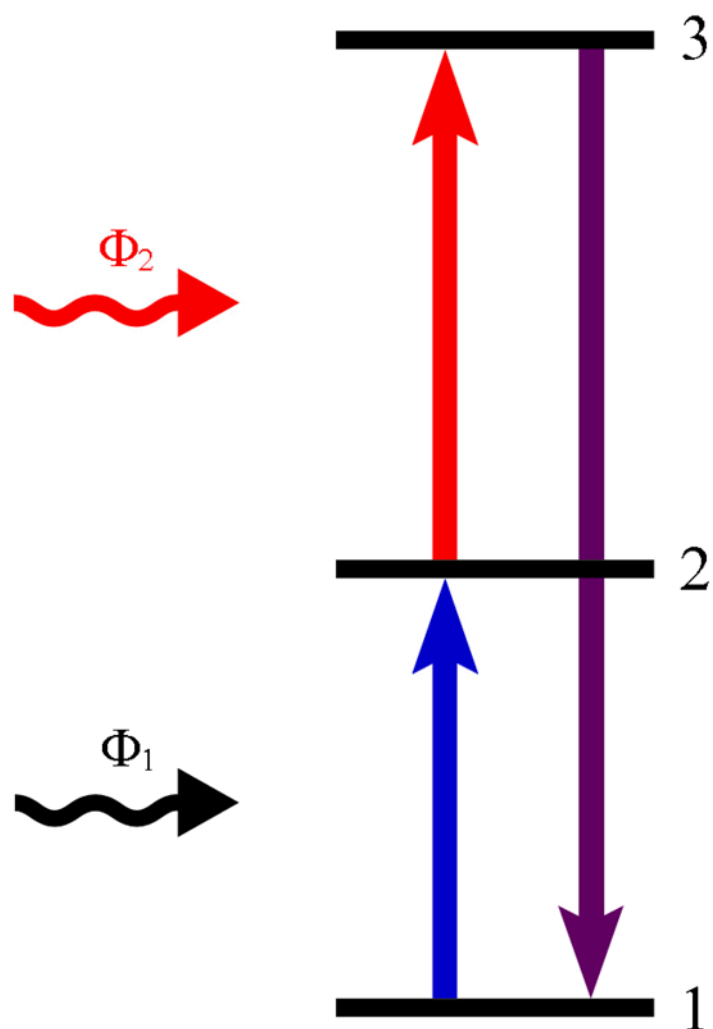
Figure 1.
General energy schemes related to the ESA process
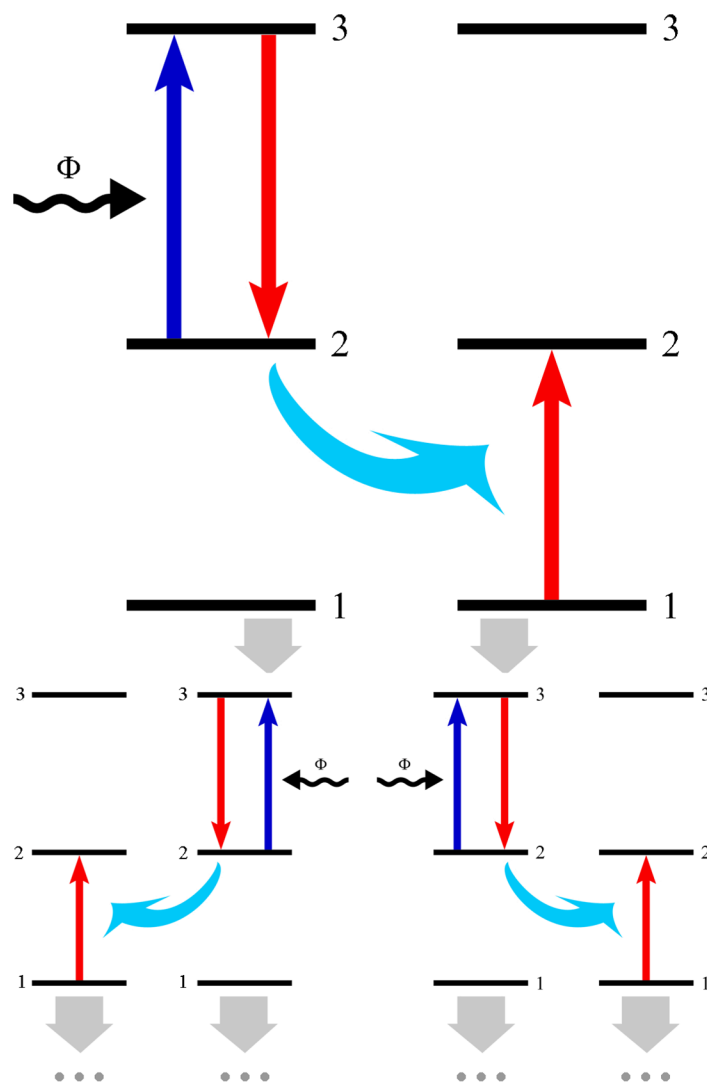
Figure 2.
General energy schemes related to the PA process
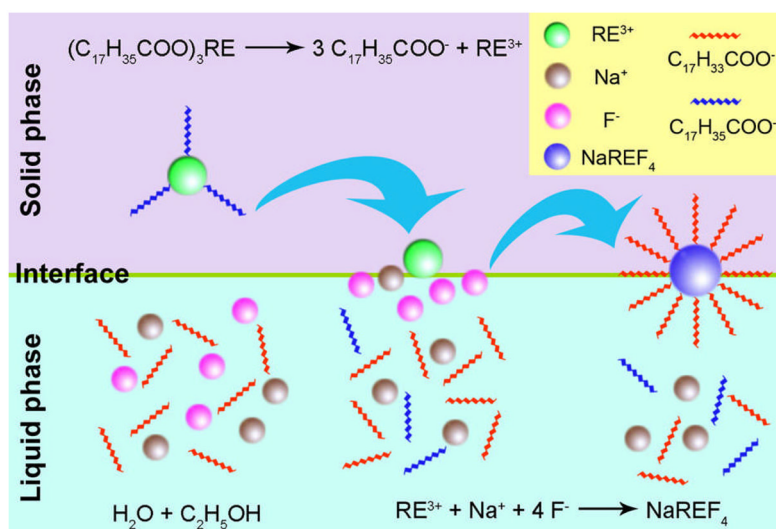
Figure 3.
Mechanism for the synthesis of NaREF$_4$ UCNPs by solvothermal method[42]
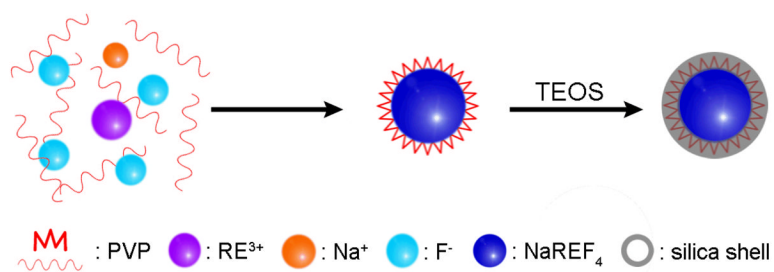
Figure 4.
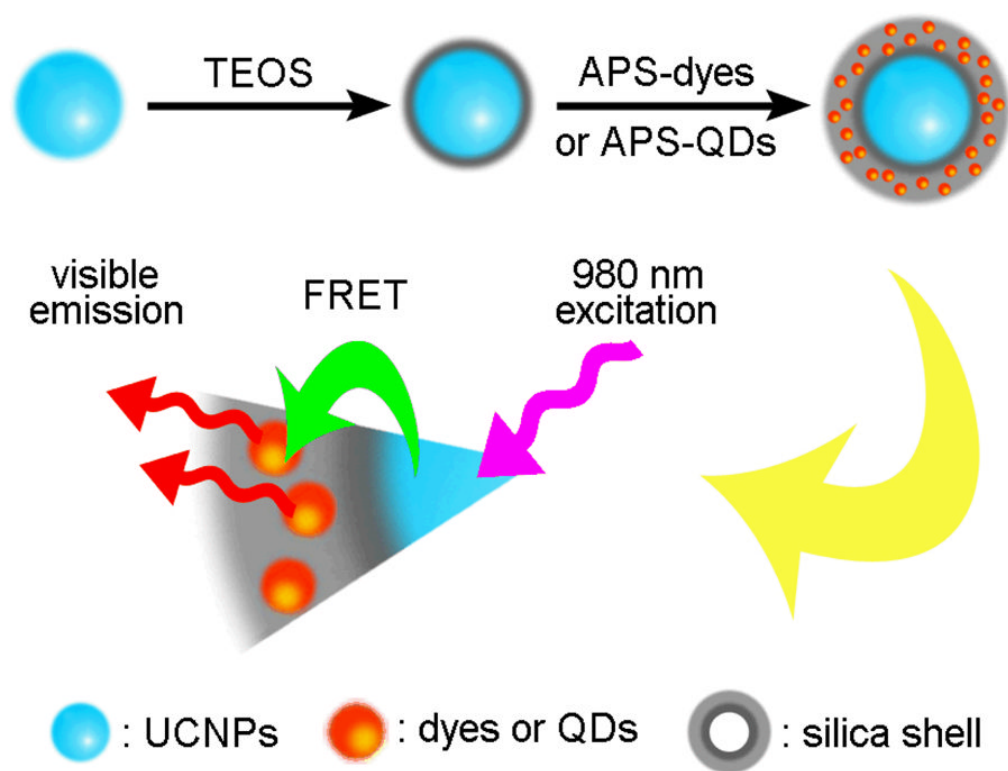Schematic illustration of the surface silica-coating of NaYF$_4$:Yb,Er@PVP UCNPs

Figure 5.
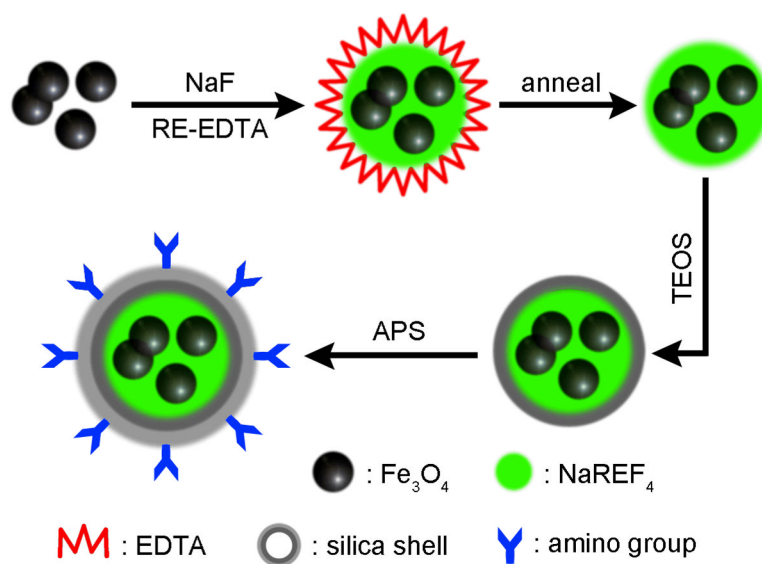Schematic illustration of silica coated multicolor UCNPs based on the FRET mechanism

Figure 6.
Schematic illustration of the modification of magnetic NaYF$_4$:Yb,Er UCNPs with silica coating
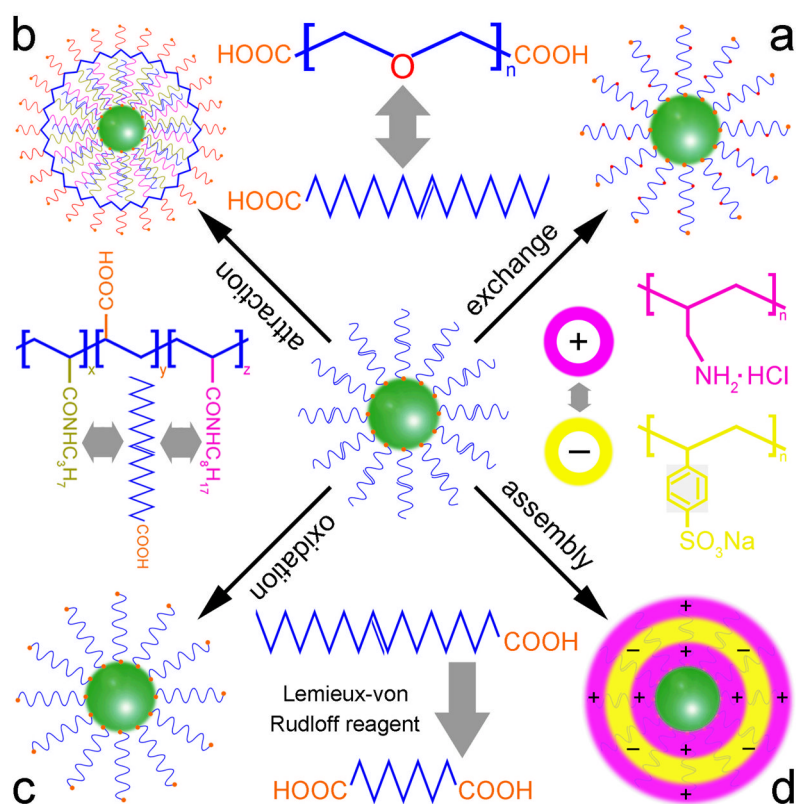
Figure 7.
The mechanisms for organic ligand modification of UCNPs: (a) ligand exchange, (b) ligand attraction, (c) ligand oxidation, and (d) ligand assembly

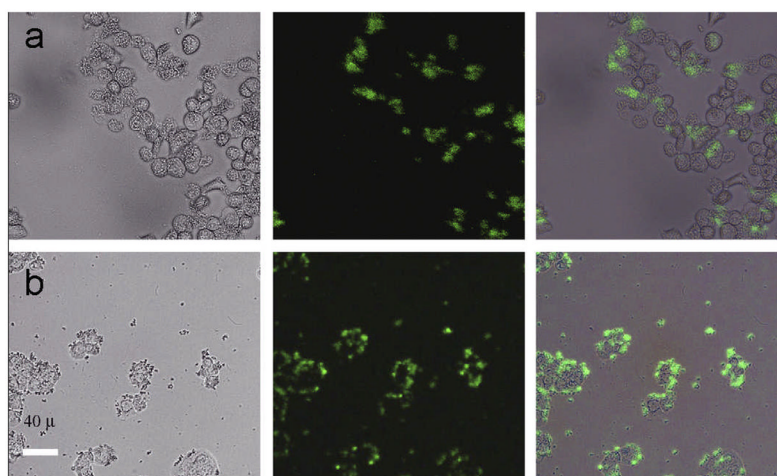**Figure 8.**
Fluorescent images of live human ovarian carcinoma cells (OVCAR3, top row) and human colonic adenocarcinoma cells (HT29, bottom row) after incubation with folic acid modified PEI/NaYF$_4$ UCNPs. The left rows are images in bright field, the middle rows are fluorescent images in dark field, and the right rows are overlays of the left and middle rows[111]
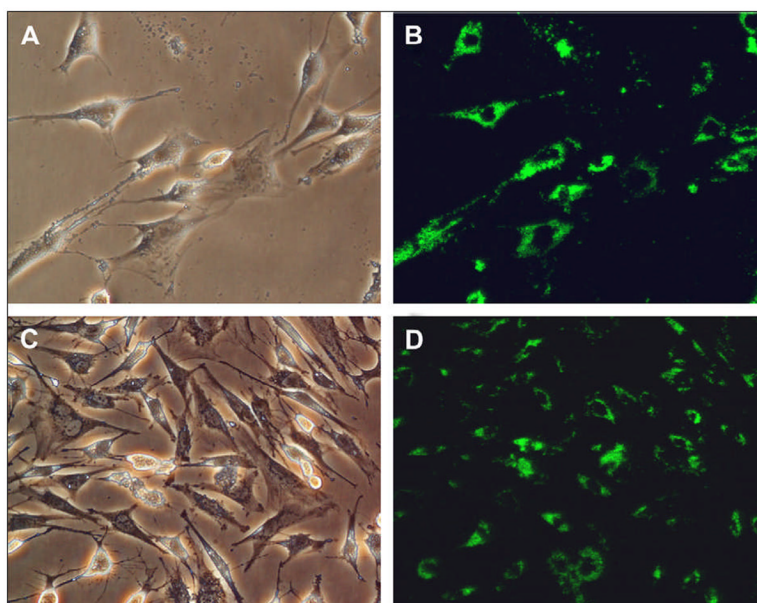
Figure 9.
Bright field (left) and fluorescent (right) images of bone marrow-derived mesenchymal stem cells (A, B) and skeletal myoblasts (C, D) treated with silica coated NaYF$_4$:Yb,Er UCNPs[112]
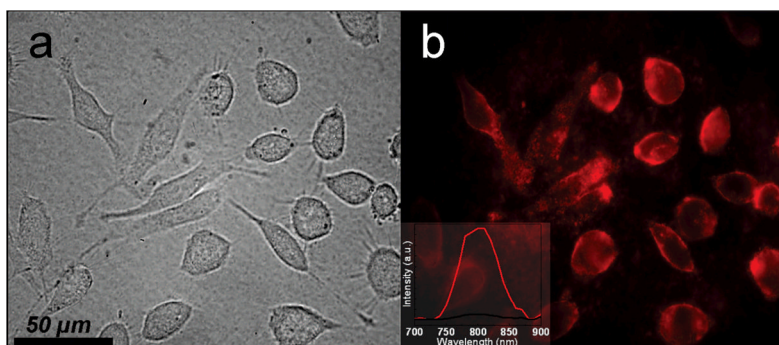
Figure 10.
Bright field (a) and fluorescence (b) images of Panc 1 cells treated with $NaYF_4$:Yb,Tm
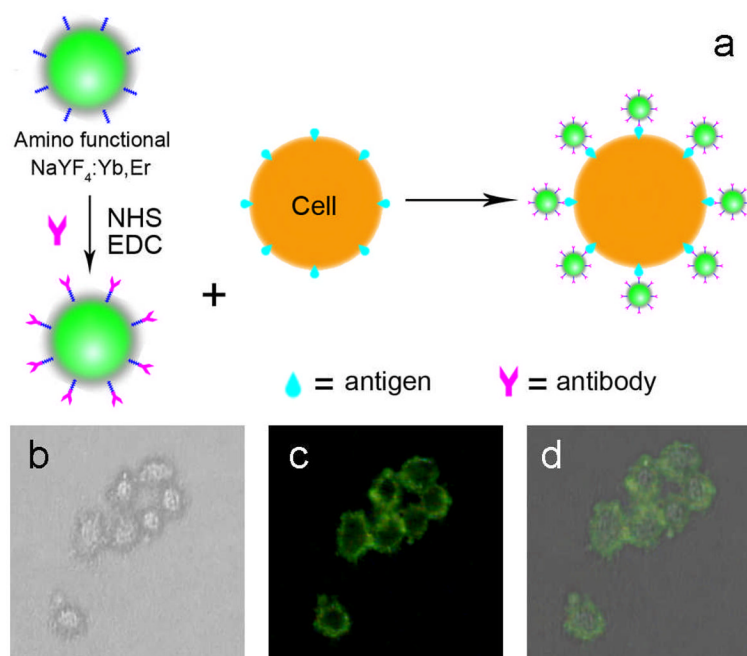UCNPs[113]

Figure 11.
Mechanism for the immunolabeling of HeLa cells using rabbit anti-CEA8 antibody conjugated $NaYF_4$:Yb,Er NPs (a), and fluorescent images of HeLa cells after incubation with rabbit anti-CEA8 antibody conjugated $NaYF_4$:Yb,Er NPs (b–d). The left row (b) is an image in bright field, the middle row (c) is an image in dark field, and right row (d) are the overlays of the left and middle rows[114]
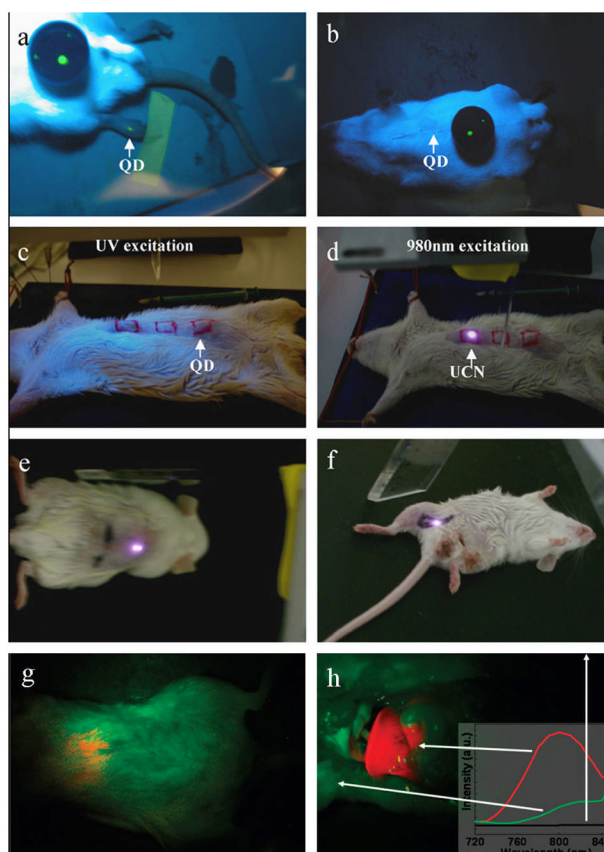
Figure 12.
In vivo imaging of rats: QDs injected into the translucent skin on the foot (a) shows fluorescence, but not through the thicker skin of the back (b) or abdomen (c); PEI/NaYF$_4$:Yb,Er UCNPs injected below the abdominal skin (d), thigh muscles (e), or below the skin of the back (f) show luminescence.[111] Whole body images of a rat iv injected with NaYF$_4$:Yb,Tm UCNPs; intact rat (g), same rat after dissection (h)[113]
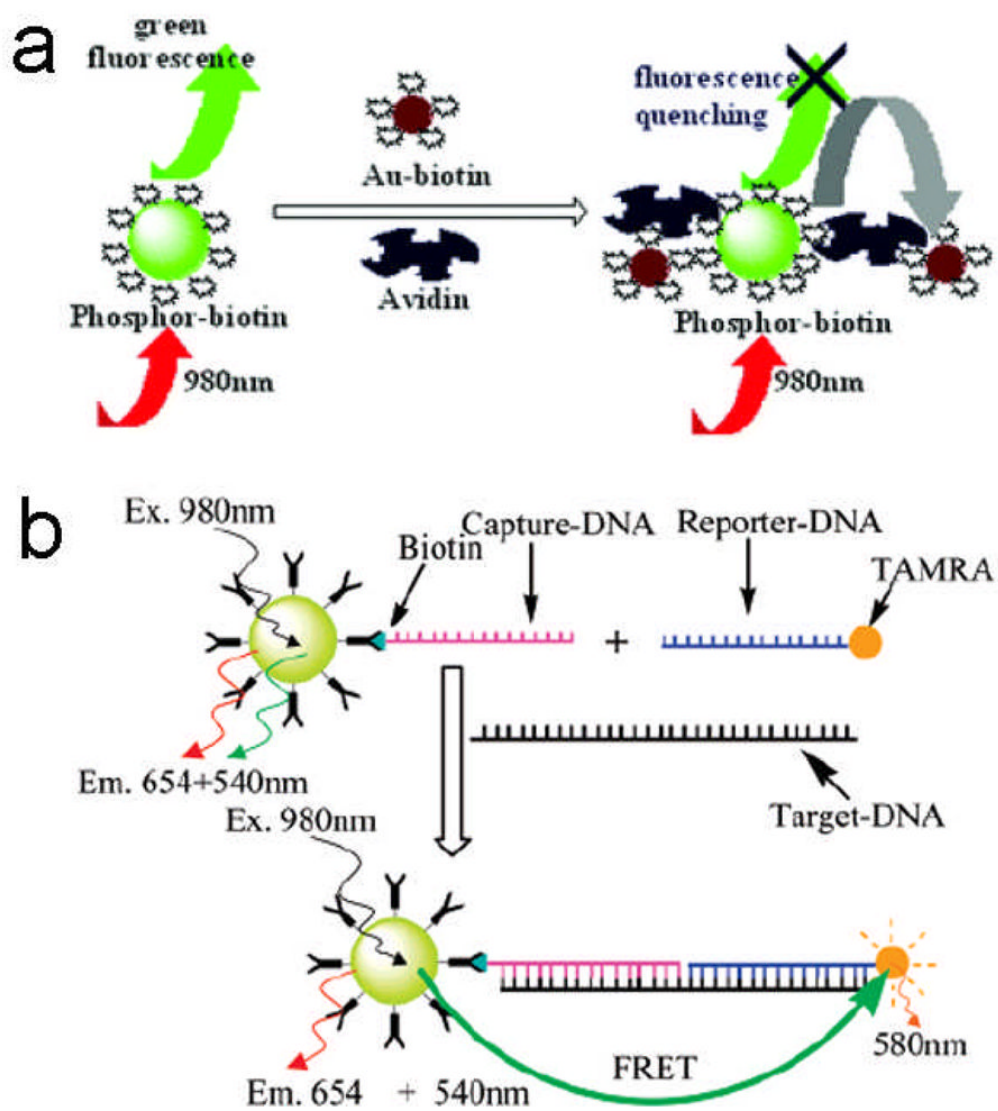
Figure 13.
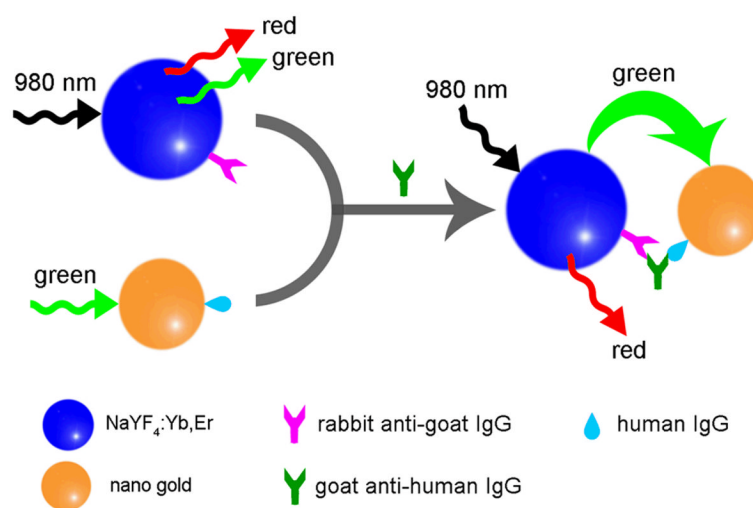FRET-based detection of (a) avidin[109] and (b) DNA[108] using the NaYF$_4$:Yb,Er UCNPs

Figure 14.
Mechanism for the LRET process between NaYF$_4$:Yb,Er UCNPs and gold NPs[121]
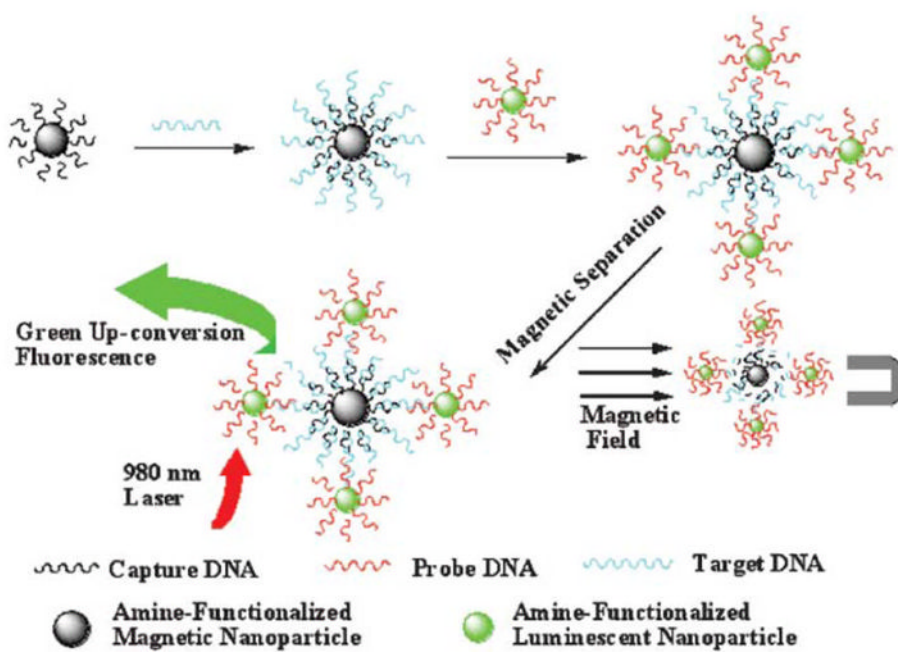
Figure 15.
Magnetic separation-based detection of DNA using NaYF$_4$:Yb,Er UCNPs[122]

Table 1

Several types of ET processes

Types	Schematic of strategies	Remarks
EFE		Energy is transferred from the sensitizing ion from an excited state to the activating ion in its state 1 by an ET, promoting the activating ion to its state 2. Next, the activating ion is promoted to its state 3 through an ESA.
SET		The activating ion in state 1 is promoted to its state 2 by an ET. Next, an activating ion is promoted again to its state 3 via a second ET. Only the sensitizing ion can absorb photos from the incident light.
CR		The sensitizing ion and the activating ion are identical ions. Photons from the incident light are absorbed by both ions, promoting these ions into state 2. An ET then promotes the activating ion to its state 3 while the sensitizing ion goes into its lower energy state.
CS		The energy accumulated from two sensitizing ions in their respective excited states is transferred to a single activating ion, promoting the activating ion to its higher excited state.
CL		The emission comprises a single process of one photon from two excited interacting ions which act as both the sensitizing ion and the activating ion.

Table 2

Different UCNPs and their luminescent properties

Host matrix	Sensitizer/activator	Emissions (nm)	Ref.
Oxide			
Y_2O_3	Yb/Er	660	17
	Yb/Tm	450, 480	19
	Yb/Ho	549, 666	21
Lu_2O_3	Yb/Er	662	22
	Yb/Tm	477, 490	22
La_2O_3	Yb/Er	530, 549, 659, 672	24
Gd_2O_3	Yb/Er	520–580, 650–700	26
Oxysulfide			
Y_2O_2S	Yb/Er	520–560, 650–680	28
	Yb/Tm	450–500, 650, 690	28
Gd_2O_2S	Yb/Er	520–580, 650–700	31
La_2O_2S	Yb/Pr	500, 508, 830	33
Oxyhalide			
GdOF	Yb/Er	521, 545, 659	36
YOF	Yb/Er	525, 545, 656	38
Phosphate			
$LaPO_4$	Yb/Er	535–556	40
$LuPO_4$	Yb/Tm	476	42
Molybdate			
$La_2(MoO_4)_3$	Yb/Er	519, 541	45
	Yb/Tm	472, 647	47
tungstate			
$NaY(WO_4)_2$	Yb/Er	526, 553, 660	18
	Yb/Tm	476, 647	20
gallate			
$Gd_3Ga_5O_{12}$	Yb/Tm	454,484, 640–680	23
vanadate			
YVO_4	Yb/Er	547, 554, 660–670	25
fluoride			
LaF_3	Yb/Er	521, 545, 659	27
	Yb/Tm	475, 698, 800	29

Host matrix	Sensitizer/activator	Emissions (nm)	Ref.
	Yb/Ho	541, 643	[30]
YF_3	Yb/Er	411, 526, 552, 664	[32]
	Yb/Tm	347, 363, 454, 477	[34]
LuF_3	Yb/Tm	481	[35]
$NaYF_4$	Yb/Er	525, 547, 660	[37]
	Yb/Tm	450, 476	[39]
	Yb/Ho	541	[39]
$LiYF_4$	Yb/Tm	361, 450, 479, 647	[41]
$NaGdF_4$	Yb/Ho	541, 647, 751	[43]
KY_3F_{10}	Yb/Er	522, 545, 656	[44]
KGd_2F_7	Yb/Er	525, 552, 666	[46]
$BaYF_5$	Yb/Tm	475, 650, 800	[48]

Table 3

Cytotoxicity data on UCNPs to different cells

cells	nanoparticles (NPs)	NPs concentration/incubation time	cell viability	Ref.
BMS cells [1]	NaYF$_4$:Yb,Er@PEI	1 µg/ml for 24–48 h	~100%	111
		25 µg/ml for 24–48 h	>90%	111
BMS cells	NaYF$_4$:Yb,Er@SiO$_2$	25 µg/ml for 24 h	91.1%	112
skeletal myoblasts	NaYF$_4$:Yb,Er@SiO$_2$	50 µg/ml for 24 h	93.3%	112
Panc 1 cells [2]	NaYF$_4$:Yb,Tm	2 mg/ml for 10 min	>90%	113
SK-BR-3 cells	NaYF$_4$@Ab-siRNA[3]	50 µg/ml for 24 h	98.6%	116
		80 µg/ml for 24 h	92.5%	116
human osteosarcoma cells	NaYF$_4$:Yb,Er@SiO$_2$	1 mg/ml for 9 days	96.2%	117
	NaYF$_4$:Yb,Er@PAA	1 mg/ml for 9 days	92.8%	117
KB cells [4]	LaF$_3$:Yb,Ho@mPEG[5]	125 µg/ml for 12 h	>85%	118
		250 µg/ml for 12 h	>80%	118
KB cells	NaYF$_4$:Yb,Tm@PAA	6–480 µg/ml for 24 h	>94%	119
		480 µg/ml for 48 h	>80%	119

[1] bone marrow-derived stem cells

[2] human pancreatic cancer cells

[3] anti-Her2 antibody conjugated NaYF4 UCNPs with siRNA attached

[4] human nasopharyngeal epidermal carcinoma cell line

[5] mPEG = polyethylene glycol monomethyl ether